Available online at www.sciencedirect.com
SCIENCE DIRECT®
Journal of Organometallic Chemistry 678 (2003) 15–32
Journal of Organometallic Chemistry
www.elsevier.com/locate/jorganchem

Facile synthesis of a novel class of organometalloid-containing ligands, the sila-β-diketones: preparation and physical and structural characterization of the copper(II) complexes, $Cu[R'C(O)CHC(O)SiR_3]_2$

Kulbinder K. Banger, Silvana C. Ngo, Seiichiro Higashiya, Rolf U. Claessen, Kenneth S. Bousman, Poay N. Lim, Paul J. Toscano *, John T. Welch *

Department of Chemistry, The University at Albany, State University of New York, 1400 Washington Avenue, Albany, NY 12222, USA

Received 31 January 2003; received in revised form 28 April 2003; accepted 28 April 2003

Abstract

The substitution of a carbon atom by silicon provides an attractive, novel approach to modification of the thermal stability and volatility of metal-organic chemical vapor deposition precursors supported by β-diketonate ancillary ligands. The low temperature reaction of the lithium enolates of acetyltrialkylsilanes with acyl chlorides affords the sila-β-diketones, $R'C(O)CH_2C(O)SiR_3$ (R′ = Me, Et, *n*-Pr, *i*-Pr, *n*-Bu, *i*-Bu, *s*-Bu, *t*-Bu; $SiR_3 = SiMe_3$, $SiEt_3$, $SiMe_2$(*t*-Bu), $SiMe_2$(*t*-hexyl), Si(*i*-Pr)$_3$), in good yields. Multinuclear NMR studies suggest that the sila-β-diketones exist as the enolic tautomer with a vinylsilane isomeric structure. Homoleptic Cu(II) sila-β-diketonate complexes were prepared in a first pass study to evaluate how precursor performance is affected by modulation of the peripheral substituents in the ligands. Thermal analyses, (TGA, DSC) show that the silylated Cu(II) precursors ($SiR_3 = SiMe_3$; R′ = *t*-Bu or *i*-Bu) have greater volatility than the corresponding carbon analogues. Some of the new Cu(II) complexes exist as liquids or low melting solids, which are preferred states for industrial deposition processes. X-ray diffraction studies of selected copper complexes showed them to have typical, square planar geometry; calculations of molecular volumes suggest that packing in the solid-state is less efficient for the silicon-containing complexes than for the non-silylated analogues.

Keywords: Sila-β-diketone; Copper complexes; Volatile complexes; Thermal analyses; Crystal structure; Chemical vapor deposition

1. Introduction

Metal-organic chemical vapor deposition (MOCVD) is widely used for the growth of epitaxial thin-films in the fabrication of computer chips, solar cells, electroluminescent displays, lasers, sensors, and superconductors [1–7]. The design criteria for MOCVD precursors can be divided into two broad categories that depend upon the application: those required for delivery of pure films at low temperature (e.g., for interconnects), and those required for co-deposition of multiple elements on one substrate, (e.g., for electro-luminescent devices).

The suitability of a precursor for MOCVD is determined by a balance of intrinsic properties, such as vapor pressure, decomposition temperature, ease of handling, and adsorption/desorption behavior of the precursor, as well as the chemical reaction pathway of the process and the purity and rate of formation of the desired thin film [1–4,8,9]. Clearly, sensible design and selection of MOCVD precursors play a significant role in the success of a particular MOCVD process. For example, many precursors currently employed or which, due to their high volatility, have been investigated as potential precursors for MOCVD of copper, contain highly fluorinated β-diketonate ligands [5,8–11], such as hfac

* Corresponding authors. Tel.: +1-518-442-3127; fax: +1-518-442-3462 (P.J.T.).
E-mail addresses: ptoscano@csc.albany.edu (P.J. Toscano), jwelch@uamail.albany.edu (J.T. Welch).

0022-328X/03/$ - see front matter © 2003 Elsevier Science B.V. All rights reserved.
doi:10.1016/S0022-328X(03)00393-0

(1,1,1,5,5,5-hexafluoropentane-2,4-dionate) or tdf (1,1,1,2,2,3,3,7,7,8,8,8,9,9,9-tetradecafluorononane-4,6-dionate) [5,12]. The hfac ligand has become a common building block in MOCVD precursor design, in spite of the inherent limitations associated with its restricted functionality, the potential for fluorine contamination of the thin film [13], and potential environmental concerns from fluorinated byproduct formation [14]. Modification of hfac to accommodate differing CVD process parameters is not economically viable or easily achieved. Substitution of fluorine by hydrocarbyl groups is not only problematic, but can also compromise volatility, while affording only minimal variation of the electronic performance of the ligand [9]. However, ternary copper(I) complexes, [Cu(hfac)(L)], which are generally air and moisture sensitive, but which permit variation of L, are often employed [1,5]. Unfortunately, Cu(I) precursors can undergo disproportionation reactions, leading to a loss of 50 mol.% of the available metal in MOCVD copper processes [5,15].

Recently, we have communicated that $Cu(tmshd)_2$ (tmshd = 2,2,6,6-tetramethyl-2-silaheptane-3,5-dionate; compound **9h** in this report), which contains a trimethylsilyl ($SiMe_3$) group, is significantly more volatile than its analogous non-silylated derivative, $Cu(tmhd)_2$ (tmhd = 2,2,6,6-tetramethylheptane-3,5-dionate) and that it is a viable precursor for copper MOCVD processes [16,17]. Presumably, the increased volatility of the former complex arises in part from the longer Si–C bonds in the $SiMe_3$ substituent as compared to the shorter C–C bonds in the latter. Further, the oxophilicity of silicon might reduce oxygen contamination of the resultant thin films by formation of volatile oxysilanes, should adverse fragmentation of the silylated ligand occur during deposition. Thus, the new sila-β-diketone, tmshdH (compound **3h** hereafter in this report), is the prototype of a new class of ligands, which provide another simple, yet effective method to tailor the performance of MOCVD precursors containing ancillary β-diketonate ligands.

In this paper, we report on the facile, general synthesis of sila-β-diketones, $R'C(O)CH_2C(O)SiR_3$ (R′ = Me, Et, *n*-Pr, *i*-Pr, *n*-Bu, *i*-Bu, *s*-Bu, and *t*-Bu; $SiR_3 = SiMe_3$, $SiEt_3$, $SiMe_2$(*t*-Bu), $SiMe_2$(*t*-hexyl), and $Si(i\text{-}Pr)_3$), as well as the homoleptic Cu(II) complexes derived therefrom. The synthetic method is sufficiently flexible to allow easily the variation of both the R′ and SiR_3 substituents in order to modify the steric and electronic properties of the new ligands. The new complexes have been characterized by thermal techniques to assess their potential usefulness in CVD applications. Also, many complexes were crystallized and studied by X-ray diffraction methods, in order to search for correlations between volatility and solid-state packing.

2. Results and discussion

2.1. Synthesis and characterization

Retrosynthetic analysis of the sila-β-diketone framework (Fig. 1) suggests that there are three possible disconnections. Relatively few reports of the preparation of this class of compound are extant [18–21]; these generally require the nucleophilic attack by a trialkylsilyl anion at an electron deficient center (disconnection between the α-trialkylsilyl group and β-carbonyl carbon atom), such as those found in substituted diketenes [18], ketoesters [19], or in more novel reagents [20,21]. Yields of the desired compounds were generally low; for example, the reaction of trimethylsilyllithium with β-ketoesters gave $<5\%$ of the target sila-β-diketone, presumably due to incomplete formation, as well as lack of regio- and chemoselectivity, of the trialkylsilyl anion [19].

Condensation of 2-trimethylsilyl-1,3-dithiane anion with an α-bromoketone, such as 1-bromo-3,3-dimethyl-2-butanone, was explored by us (disconnection between γ-carbon atom and β-carbonyl carbon; Fig. 1) and will be reported elsewhere [22]. Unmasking of the protected carbonyl functionality by the action of $HgCl_2$/HgO did afford the sila-β-diketone **3h**, albeit in low to modest overall yield.

However, a synthetic method (Schemes 1 and 2) based upon disconnection between the γ-carbon atom and the β′-carbonyl carbon bearing the putative non-silylated substituent (Fig. 1) proved to be the most versatile strategy, due to the ready commercial availability of acyl chlorides R′C(O)Cl (R′ = Me (**1a**), Et (**1b**), *n*-Pr (**1c**), *i*-Pr (**1d**), *n*-Bu (**1e**), *i*-Bu (**1f**), *s*-Bu (**1g**), and *t*-Bu (**1h**)), shorter reaction times, and the overall generality of the procedure. Acylsilanes $MeC(O)SiR_3$ ($SiR_3 = SiMe_3$ (**2a**), $SiEt_3$ (**2b**), $SiMe_2$(*t*-Bu) (**2c**), $SiMe_2$(*t*-hexyl) (**2d**), and $Si(i\text{-}Pr)_3$ (**2e**)) were easily prepared by reaction of the appropriate chlorotrialkylsilane with lithiated ethyl vinyl ether at low temperature, followed by acid catalyzed hydrolysis of the intermediate silylated enol ether (Scheme 1) [23,24].

The low temperature (−85 °C) reaction of the lithium enolate of an acetyltrialkylsilane (**2a**–**e**) with an acyl chloride (**1a**–**h**) provided a general, scalable route for the synthesis of sila-β-diketones (**3**–**7**) (see Scheme 2 for the numbering convention which indicates the substitu-

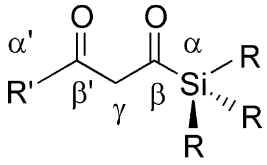

Fig. 1. Schematic drawing with labeling of carbon atoms for a general sila-β-diketone.

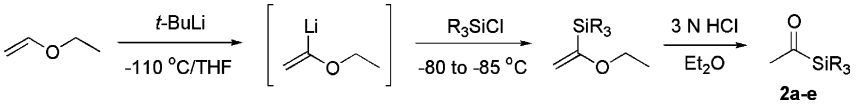

Scheme 1. General preparation of acetyltrialkylsilanes **2a**–**e**.

ents present on the sila-β-diketone compounds). In general, while the reaction yields were not optimized, they were acceptable (ca. 40–70%). The yields were likely compromised by side reactions, such as *O*-silylation, β-proton abstraction, and self-condensation reactions. From the presumed loss of selectivity as the relative amounts of byproducts formed in the preparations of **3**–**7** increased as judged by chromatographic methods, we could deduce the trend of reactivity for the lithium enolates, as a function of the trialkylsilyl substituent: $SiMe_3 > > > SiMe_2(t\text{-Bu}) > SiEt_3 > SiMe_2(t\text{-hexyl}) > Si(i\text{-Pr})_3$.

In the case of the more reactive $SiMe_3$-containing intermediate, a range of reaction conditions was investigated in order to minimize these alternate reaction pathways. We found that utilization of a 1:1:1 ratio of reactants (LDA/$MeC(O)SiMe_3$ (**2a**)/acyl chloride) at $-110\ ^{\circ}C$, combined with the slow addition of the enolate of **2a** to the acyl chloride, reduced the amount of undesirable byproducts. Deviation from this stoichiometric ratio resulted in significant losses to side reactions. In particular, use of excess LDA (1.5 mol equiv.) resulted in significantly lower yields of the desired sila-β-diketone. The reaction of alkyl esters, rather than acyl chlorides, with the enolate of **2a**, gave no reaction, or very poor yields ($< 10\%$) of the target compounds. Use of higher reaction temperatures was limited by the instability of the enolate of **2a**. Lastly, reverse addition of *t*-BuC(O)Cl (**1h**) to the enolate of **2a** gave a complex mixture of products. Work up of the crude orange mixture provided translucent, colorless crystals. Single crystal X-ray diffraction analysis confirmed the product **8** to be the result of a cyclic condensation of *t*-$BuC(O)CH_2C(O)SiMe_3$ (**3h**) with another unit of **2a** (Scheme 2), giving after workup 6-*t*-butyl-2,4-bis-(trimethylsilyl)tetrahydropyran-2,4-diol (Fig. 2). Most of the bond lengths and angles in **8** are unremarkable; however, the bonds from silicon to the ring carbon atoms (Si(1)–C(1) 1.915(5) and Si(2)–C(3) 1.911(5) Å) are significantly longer than the Si–Me bond lengths (avg. 1.844(7) Å) [25]. This observation may be due to the juxtaposition of two electropositive atoms in the former bonds, namely the silicon atom and a carbon atom bearing a hydroxyl substituent. The hydrogen atom bonded to O(2) is *intra*molecularly H-bonded to O(3), while the hydrogen atom bonded to O(3) is

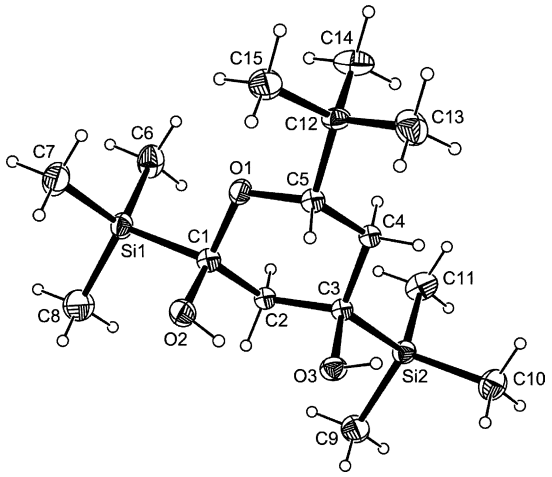

Fig. 2. Molecular structure and atom numbering scheme for **8**.

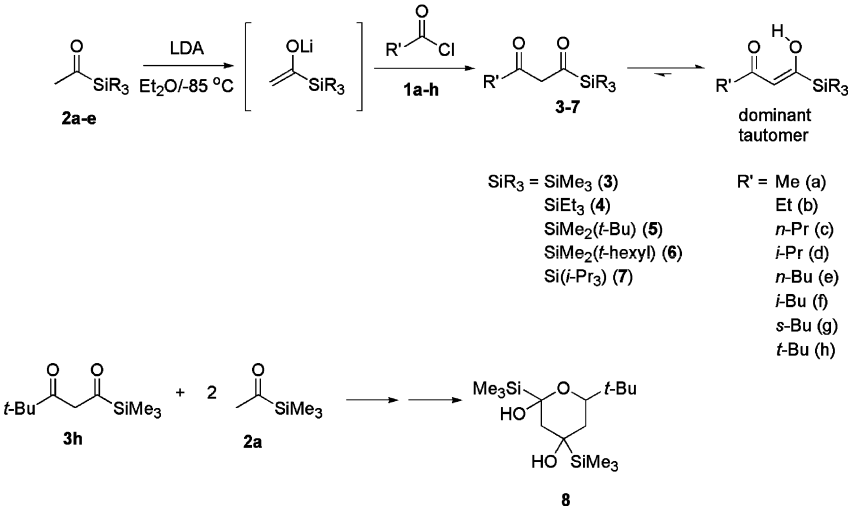

Scheme 2. General preparation of sila-β-diketones (**3**–**7**).

*inter*molecularly H-bonded to O(2) on a symmetry related molecule at $0.5-x$, $0.5-y$, $-z$. The latter interactions cause **8** to form H-bonded chains parallel to the *b* axis of the crystal.

Consistent with our previous findings, ^{1}H- and ^{13}C-NMR spectroscopy revealed that the sila-β-diketones (**3**–**7**) exist exclusively as enolic tautomers [16]. Further, we can deduce that the predominant tautomer for **3**–**7** has the vinylsilane structure (Scheme 2) based upon the ^{13}C-NMR chemical shifts (ca. 200 ppm) for the trigonal carbon atom adjacent to silicon. These numbers are considerably upfield compared to typical ^{13}C=O chemical shifts for acylsilanes (ca. 240 ppm) [23,26,27]. The NMR data for **3**–**7** are otherwise in accord with the proposed structure for this tautomer. The UV spectra of the sila-β-diketones (**3**–**7**) generally contain only one absorption at ca. 276 nm, that is slightly less intense than that for non-silylated β-diketonate analogs. The lack of the expected bathochromic shift or hyperchromic effect expected for an acylsilane is again consistent with the predominant enolic tautomer being toward silicon [16].

The homoleptic Cu(II) complexes, Cu[R′C(O)CHC(O)SiR$_3$]$_2$ (**9**–**13**), were prepared by either direct deprotonation and complexation of **3**–**7** with copper(II) acetate or by reaction of the alkali salts of **3**–**7** with copper(II) chloride in either aprotic or protic solvents (Scheme 3; this scheme also provides the numbering convention which indicates the substituents present on the sila-β-diketonate ligands of the complexes). In comparative studies, the latter methods gave higher yields of the desired complex ($>80\%$), but the former route was frequently employed, because of the moderate reaction conditions and its applicability to the use of unpurified ligands. Excess Cu(II) salt was generally employed to ensure complete reaction of the silylated ligands.

Most of the complexes were isolated as greenish solids, with the exceptions of Cu[R′C(O)CHC(O)SiEt$_3$]$_2$ (**10a**–**h**), which were found to exist as oily green liquids or low melting solids. As we have previously noted, the

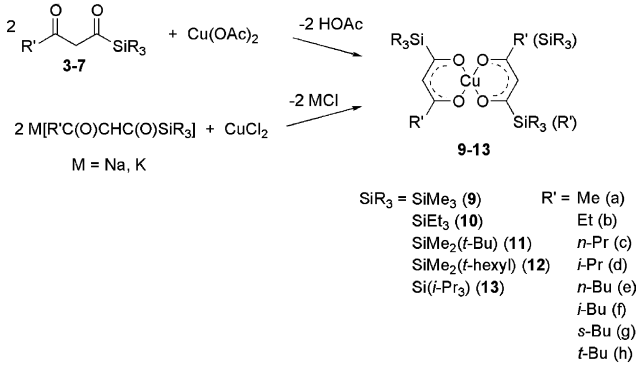

Scheme 3. Methods of synthesis of the homoleptic Cu(II) sila-β-diketonate complexes.

green coloration is generally due to a broad, moderately intense charge transfer band in the electronic spectrum that occurs at ca. 360–370 nm ($\varepsilon \sim 9000$) and which tails into the blue portion of the visible region, in combination with weak d–d transitions at ca. 520 ($\varepsilon \sim 100$) and 655 nm ($\varepsilon \sim 50$) [16].

2.2. Thermal analysis of the Cu(II) complexes

Thermogravimetric analysis (TGA) and differential scanning calorimetry (DSC) provided useful methods for establishing the extent of modulation of precursor performance as a function of variation of the substituents on either the silicon moiety at the α-position or on the alkyl group at the α′-position of the ligands (Fig. 1). The TGA traces of the series of copper complexes **9**–**13** showed rapid and complete volatilization over a narrow temperature range, with no indication of decomposition. The temperature of the maximum rate of weight loss (T_{MWL}; Table 1) was used as a measure of the relative volatilities of the complexes, since weight loss was associated with the vaporization of the complexes. The T_{MWL} values ranged from 148 °C for Cu[*i*-PrC(O)CHC(O)SiMe$_3$]$_2$ (**9d**) to a high of 223 °C for Cu[*i*-PrC(O)CHC(O)Si(*i*-Pr)$_3$]$_2$ (**13d**). On the other hand DSC provided information on the thermal stability and temperature dependent phase changes of the complexes (Table 1). The DSC samples were heated under a dinitrogen atmosphere, using hermetically sealed aluminum pans, to eliminate weight loss associated with sublimation. The decomposition values ranged from 159 °C for Cu[*i*-PrC(O)CHC(O)SiMe$_3$]$_2$ (**9d**) to a high of 245 °C for Cu[*t*-BuC(O)CHC(O)SiMe$_3$]$_2$ (**13h**). We now turn to a discussion of trends within series of compounds.

If the α-trialkylsilyl substituent is held constant, variation of the alkyl group R′ at the α′-position has little effect on decomposition temperature of the copper complexes Cu[R′C(O)CHC(O)SiR$_3$]$_2$ in that series. As expected, increasing the length of the normal carbon chain from R′ = Me (**9a**–**13a**) to *n*-Bu (**9e**–**13e**) causes an attendant decrease of the melting point. Complexes having branched R′ groups tended to have somewhat higher melting points. Volatility, as assessed by T_{MWL} values, was also only modestly affected as a function of R′. For complexes having the same molecular mass, those having an R′ group with a more branched structure tended to be slightly more volatile than those having a straight chain structure; for example, complexes Cu[*i*-PrC(O)CHC(O)SiR$_3$]$_2$ (**9d**–**13d**) were more volatile than complexes Cu[*n*-PrC(O)CHC(O)SiR$_3$]$_2$ (**9c**–**13c**). Likewise, similar results were observed in most cases for the series Cu[*i*-BuC(O)CHC(O)SiR$_3$]$_2$ (**9f**–**13f**), Cu[*s*-BuC(O)CHC(O)SiR$_3$]$_2$ (**9g**–**13g**), or Cu[*t*-BuC(O)CHC(O)SiR$_3$]$_2$ (**9h**–**13h**) vs. Cu[*n*-BuC(O)CHC(O)SiR$_3$]$_2$ (**9e**–**13e**).

Table 1
TGA and DSC data for Cu(II) sila-β-diketonate complexes **9**–**13**, $Cu[R'C(O)CHC(O)SiR_3]_2$

Cu(II) complex	R′; SiR_3	TGA		DSC	
		T_{MWL} [a] (°C)	Residue (%)	M.p. (°C)	Dec. (°C)
9a	Me; $SiMe_3$	155	4	93	189
9b	Et; $SiMe_3$	147	5	96	171
9c	*n*-Pr; $SiMe_3$	160	8	68	172
9d	*i*-Pr; $SiMe_3$	148	4	94	159
9e	*n*-Bu; $SiMe_3$	161	9	43	174
9f	*i*-Bu; $SiMe_3$	152	8	102	166
9g	*s*-Bu; $SiMe_3$	149	4	107	167
9h	*t*-Bu; $SiMe_3$	149	2	161	172
10a	Me; $SiEt_3$	185	6	47	208
10b	Et; $SiEt_3$	183	4	[b]	203
10c	*n*-Pr; $SiEt_3$	192	5	[b]	199
10d	*i*-Pr; $SiEt_3$	190	7	[b]	203
10e	*n*-Bu; $SiEt_3$	197	9	[b]	202
10f	*i*-Bu; $SiEt_3$	192	7	[b]	200
10g	*s*-Bu; $SiEt_3$	188	4	[b]	195
10h	*t*-Bu; $SiEt_3$	192	5	[b]	196
11a	Me; $SiMe_2(t\text{-Bu})$	174	2	[c]	[c]
11b	Et; $SiMe_2(t\text{-Bu})$	176	3	86	208
11c	*n*-Pr; $SiMe_2(t\text{-Bu})$	184	2	80	215
11d	*i*-Pr; $SiMe_2(t\text{-Bu})$	174	1	83	216
11e	*n*-Bu; $SiMe_2(t\text{-Bu})$	197	2	41	214
11f	*i*-Bu; $SiMe_2(t\text{-Bu})$	188	1	87	209
11g	*s*-Bu; $SiMe_2(t\text{-Bu})$	182	1	99	219
11h	*t*-Bu; $SiMe_2(t\text{-Bu})$	182	4	[c]	[c]
12a	Me; $SiMe_2(t\text{-Hx})$	202	5	76	227
12b	Et; $SiMe_2(t\text{-Hx})$	203	8	89	224
12c	*n*-Pr; $SiMe_2(t\text{-Hx})$	213	5	50	234
12d	*i*-Pr; $SiMe_2(t\text{-Hx})$	209	2	74	235
12e	*n*-Bu; $SiMe_2(t\text{-Hx})$	218	6	[b]	229
12f	*i*-Bu; $SiMe_2(t\text{-Hx})$	210	2	59	233
12g	*s*-Bu; $SiMe_2(t\text{-Hx})$	209	4	56	236
12h	*t*-Bu; $SiMe_2(t\text{-Hx})$	207	4	101	228
13b	Et; $Si(i\text{-Pr})_3$	218	3	51	231
13c	*n*-Pr; $Si(i\text{-Pr})_3$	217	5	52	236
13d	*i*-Pr; $Si(i\text{-Pr})_3$	223	3	59	236
13e	*n*-Bu; $Si(i\text{-Pr})_3$	230	9	59	234
13f	*i*-Bu; $Si(i\text{-Pr})_3$	218	8	[b]	237
13g	*s*-Bu; $Si(i\text{-Pr})_3$	215	4	75	238
13h	*t*-Bu; $Si(i\text{-Pr})_3$	217	2	68	245

[a] Temperature of maximum weight loss.
[b] Oily liquid at room temperature.
[c] DSC measurements were not performed.

On the other hand, if R′ is held constant, decomposition temperatures tend to increase as molecular mass of the α-trialkylsilyl substituent increases. Perhaps more importantly, the stability of the Cu(II) complexes increases as steric congestion at the silicon atom increases, suggesting that decomposition may begin with attack at the silicon atom. T_{MWL} values also generally increase with the molecular mass and size of the α-trialkylsilyl substituent, the notable exception being $Cu[R'C(O)CHC(O)SiMe_2(t\text{-Bu})]_2$ (**11a**–**h**). Although **11a**–**h** are ca. 7% more massive than the corresponding $Cu[R'C(O)CHC(O)SiEt_3]_2$ (**10a**–**h**), the former have lower T_{MWL} values in a number of cases.

One of the more striking observations on the ability of silicon to alter the properties of potential non-fluorinated MOCVD precursors is that $Cu[R'C(O)CHC(O)SiEt_3]_2$ (**10b**–**h**), are the first Cu(II) MOCVD precursors that are liquids at room temperature. Interestingly, dissolution of these complexes in aqueous ethanol, followed by slow evaporation at low temperatures, often yielded highly crystalline, low melting point solids. The change to solid phase may arise from coordination of solvent molecules to the Cu atom in the axial positions or, more likely, from incorporation of molecules of solvation in the crystalline lattice. The solvent molecules are lost rapidly when the crystals are

removed from the mother liquor and warmed up; application of a weak vacuum results in the rapid removal of solvent from the crystals and the expected phase transition from solid to liquid. The loss of solvent was too rapid to adequately characterize these apparent solvates.

We have previously noted that Cu[*t*-BuC(O)CHC(O)SiMe$_3$]$_2$ (**9h**) is considerably more volatile than the carbon-containing analogue, Cu(tmhd)$_2$, the former having a T_{MWL} ca. 15 °C lower than the latter [16]. We find similar results in the comparison of Cu[*i*-BuC(O)CHC(O)SiMe$_3$]$_2$ (**9f**) with Cu(tmod)$_2$ (tmod = 2,2,7-trimethyloctane-3,5-dionate). The T_{MWL} for **9f** is 20 °C lower than that for Cu(tmod)$_2$. The silylated Cu(II) complex also has a lower melting point (152 °C vs. 173 °C) and decomposes over a lower, narrower temperature range (the DSC traces of the carbon-containing analogs tend not to show a sharp decomposition point).

2.3. Single-crystal X-ray diffraction studies of selected Cu(II) complexes

In order to investigate solid-state packing effects and to better study the influence of silicon substitution on bonding parameters, 14 of the new complexes, Cu[R′C(O)CHC(O)SiR$_3$]$_2$ with various R′ and SiR$_3$ groups, were crystallized for study by X-ray diffraction methods. Previous structural results for Cu[*t*-BuC(O)CHC(O)SiMe$_3$]$_2$ (**9h**) were compromised by site-disordering effects [16]; however, in the crystals studied here, the molecules are generally well-ordered, even when the Cu atom is situated on a special position in the unit cell. We note that for a small number of cases, in which SiR$_3$ = SiEt$_3$ (**10a**) or SiMe$_2$(*t*-Bu) (**11d**, **g**, **h**), the data sets were marred somewhat by high thermal motion in the trialkylsilyl substituents. Nevertheless, we have included these compounds in the discussion for the facilitation of comparisons involving unit cell packing.

In all 14 structures, the molecular geometry is essentially square planar (however, vide infra). Selected bond lengths and angles for the Cu(II) complexes are collected in Table 2 (copper atom on general position in the unit cell) and Table 3 (copper atom on special position in the unit cell). Since the sila-β-diketonate ligands are necessarily unsymmetrically substituted, geometrical isomers are possible. Crystals of Cu[MeC(O)CHC(O)SiMe$_3$]$_2$ (**9a**) (Fig. 3), Cu[EtC(O)CHC(O)SiMe$_3$]$_2$ (**9b**), Cu[*i*-PrC(O)CHC(O)SiMe$_3$]$_2$ (**9d**), Cu[MeC(O)CHC(O)SiEt$_3$]$_2$ (**10a**) (including both crystallographically independent molecules), Cu[MeC(O)CHC(O)SiMe$_2$(*t*-Bu)]$_2$ (**11a**), and Cu[*t*-BuC(O)CHC(O)SiMe$_2$(*t*-Bu)]$_2$ (**11h**) contain molecules of *cis*-geometry, while Cu[*i*-BuC(O)CHC(O)SiMe$_3$]$_2$ (**9f**), Cu[*i*-PrC(O)CHC(O)SiMe$_2$(*t*-Bu)]$_2$ (**11d**) (including both crystallographically independent molecules), Cu[*i*-BuC(O)CHC(O)SiMe$_2$(*t*-Bu)]$_2$ (**11f**) (Fig. 4), Cu[*s*-BuC(O)CHC(O)SiMe$_2$(*t*-Bu)]$_2$ (**11g**), Cu[EtC(O)CHC(O)Si(*i*-Pr)$_3$]$_2$ (**13b**), and Cu[*t*-BuC(O)CHC(O)Si(*i*-Pr)$_3$]$_2$ (**13h**) have the *trans* configuration. In one case, Cu[*n*-PrC(O)CHC(O)SiMe$_3$]$_2$ (**9c**), we serendipitously identified crystals that *separately* contained each isomer, which we have designated as **9c**-*cis* and **9c**-*trans*, respectively. We believe that both geometrical isomers are likely present in bulk samples of all the complexes and that either spontaneous separation or interconversion of isomers occurs during the crystallization process [28]. We note that Ripmeester and coworkers have previously isolated different crystals of Cu[F$_3$CC(O)CHC(O)CMe$_2$(OMe)]$_2$ that contained, respectively, only *trans*-isomer and a mixture of *cis*- and *trans*-isomers [29].

Bond lengths and angles within the coordination spheres are similar to those for disordered Cu[*t*-BuC(O)CHC(O)SiMe$_3$]$_2$ (**9h**) [16] and for other non-silylated Cu(II) complexes with ancillary β-diketonate ligands having large peripheral substituents [28,30–32]. As expected, the *trans* O–Cu–O bond angles deviate somewhat more from linearity for those complexes in which a distortion from square planar geometry occurs (vide infra).

Disorder problems involving the peripheral *t*-Bu and SiMe$_3$ substituents for Cu[*t*-BuC(O)CHC(O)SiMe$_3$]$_2$ (**9h**) precluded detailed discussion on the effect of silicon substitution on bond lengths and angles involving the ligands of the complexes [16]. We can say more confidently, based on the present results, that silicon substitution does not appear to have any significant effect on bonding parameters within the chelate rings of the β-diketonate ligands. Complex Cu[MeC(O)CHC(O)SiMe$_3$]$_2$ (**9a**) (Fig. 3) arguably provided the best data; for **9a**, the C(1)–C(2) and C(8)–C(9) bond distances (toward the R′ side of the ligands) are 1.397(2) and 1.405(4) Å, respectively, while C(2)–C(3) and C(9)–C(10) bond distances (toward the SiR$_3$ side of the ligands) are 1.392(4) and 1.378(3) Å, respectively. Similar results are observed for all the other nine complexes, which were not marred by high thermal motion in the SiR$_3$ substituents. However, the bond distances from silicon to the carbonyl carbon of the chelates are, in general, longer (by 0.05–0.08 Å) than the silicon to sp^3-carbon atoms within the SiR$_3$ units. The elongation of the Si–C(O) bond in acylsilanes has been ascribed previously to the contribution of a resonance structure having no formal bond between silicon and the carbonyl carbon [33,34]; alternatively, the bond lengthening might occur in response to the electropositive nature of the two atoms comprising the bond.

The chelate rings in the complexes are all very nearly planar, with the largest deviation from planarity being only ±0.051 Å for the ring including O(3) and O(4) for

Table 2
Selected bond lengths (Å) and angles (°) for Cu[MeC(O)CHC(O)SiMe$_3$]$_2$ (**9a**), Cu[EtC(O)CHC(O)SiMe$_3$]$_2$ (**9b**), Cu[*n*-PrC(O)CHC(O)SiMe$_3$]$_2$ (**9c**-*cis* and **9c**-*trans*), Cu[*i*-BuC(O)CHC(O)SiMe$_3$]$_2$ (**9f**), Cu[MeC(O)CHC(O)SiEt$_3$]$_2$ (**10a**), Cu[MeC(O)CHC(O)SiMe$_2$(*t*-Bu)]$_2$ (**11a**), and Cu[EtC(O)CHC(O)Si(*i*-Pr)$_3$]$_2$ (**13b**)

	9a	**9b**	**9c**-*cis*	**9c**-*trans*	**9f**
Bond lengths					
Cu(1)–O(1)	1.913(2)	1.918(4)	1.911(5)	1.920(8)	1.911(4)
Cu(1)–O(2)	1.912(2)	1.905(4)	1.903(4)	1.913(8)	1.903(5)
Cu(1)–O(3)	1.916(2)	1.909(4)	1.917(5)	1.909(8)	1.904(5)
Cu(1)–O(4)	1.917(2)	1.906(3)	1.897(5)	1.911(9)	1.905(5)
Bond angles					
O(1)–Cu(1)–O(2)	93.7(1)	94.2(2)	93.5(2)	93.2(3)	93.7(2)
O(1)–Cu(1)–O(3)	85.5(1)	86.4(2)	86.1(2)	171.4(3)	173.7(3)
O(1)–Cu(1)–O(4)	177.2(1)	163.2(2)	178.1(2)	86.9(3)	85.6(2)
O(2)–Cu(1)–O(3)	178.3(1)	163.2(2)	173.7(2)	88.9(3)	88.7(2)
O(2)–Cu(1)–O(4)	87.5(1)	90.2(2)	87.7(2)	165.5(3)	168.4(2)
O(3)–Cu(1)–O(4)	93.4(1)	94.0(2)	92.6(2)	93.2(4)	93.1(2)
	10a/molec 1 [a]	**10a**/molec 2 [a]	**11a**	**13b**	
Bond lengths					
Cu(1)–O(1)	1.90(1)	1.97(2)	1.903(4)	1.920(4)	
Cu(1)–O(2)	1.91(2)	1.89(2)	1.907(4)	1.893(3)	
Cu(1)–O(3)	1.91(2)	1.92(2)	1.918(4)	1.920(4)	
Cu(1)–O(4)	1.91(1)	1.92(2)	1.894(4)	1.897(3)	
Bond angles					
O(1)–Cu(1)–O(2)	93.5(7)	92.9(8)	93.9(2)	93.2(2)	
O(1)–Cu(1)–O(3)	85.2(7)	85.4(8)	85.9(2)	175.2(2)	
O(1)–Cu(1)–O(4)	171.9(7)	170.7(6)	177.5(2)	86.4(2)	
O(2)–Cu(1)–O(3)	177.6(6)	175.6(7)	170.6(2)	87.5(2)	
O(2)–Cu(1)–O(4)	87.3(7)	88.5(8)	87.3(2)	175.4(2)	
O(3)–Cu(1)–O(4)	93.8(7)	93.8(8)	92.3(2)	93.2(2)	

[a] There are two crystallographically independent molecules in the asymmetric unit of **10a**.

Cu[MeC(O)CHC(O)SiMe$_3$]$_2$ (**9a**). Dihedral angles between the chelate rings in the complexes are 5.1(1)° (Cu[MeC(O)CHC(O)SiMe$_3$]$_2$ (**9a**)), 24.0(2)° (Cu[EtC(O)CHC(O)SiMe$_3$]$_2$ (**9b**)), 5.5(3)° (Cu[*n*-PrC(O)CHC(O)SiMe$_3$]$_2$ (**9c**-*cis*)), 17.0(5)° (**9c**-*trans*), 13.5(3)° (Cu[*i*-BuC(O)CHC(O)SiMe$_3$]$_2$ (**9f**)), 4.1(9)° (Cu[MeC(O)CHC(O)SiEt$_3$]$_2$ (**10a**), independent molecule 1), 13.2(9)° (**10a**, independent molecule 2), 9.7(2)° (Cu[MeC(O)CHC(O)SiMe$_2$(*t*-Bu)]$_2$ (**11a**)), 3.2(6)° (Cu[*t*-BuC(O)CHC(O)SiMe$_2$(*t*-Bu)]$_2$ (**11h**)), and 6.5(2)° (Cu[EtC(O)CHC(O)Si(*i*-Pr)$_3$]$_2$ (**13b**)); for the remainder of the molecules studied, the Cu atom is situated on a special position, that enforces a dihedral angle of 0.0°. Clearly, there is a continuum of values ranging from 0.0° to a rather large twist angle for **9b**. In the majority of the cases where the dihedral angle is nonzero, the twisting appears to allow maximum overlap of chelate rings between crystallographic neighbors; distances between ring centroids range from 3.193 to 3.381 Å. For **9a** and **9b**, the peripheral substituent groups are apparently small enough so that stacking occurs along an 'inclined' line [31] parallel to the *a* axis for the former compound and parallel to the *b* axis for the latter. For **9c**-*cis*, **9c**-*trans*, **9f**, **10a**, and **11a**, overlap occurs only between *pairs* of crystallographically related molecules. The remainder of the structurally characterized molecules only exhibit van der Waals interactions between the Cu centers and peripheral C–H groups or between alkyl groups, the latter of which are generally present for all the complexes. While there seems to be a strong preference for stacking interactions to occur, if sterically possible, the rather modest decrease in T_{MWL} values as a function of R′ as the α-trialkylsilyl is held constant suggests that the presence of chelate ring overlaps in the solid-state structure is not a major contributor to loss of volatility.

We have reported previously that the calculated density of Cu[*t*-BuC(O)CHC(O)SiMe$_3$)]$_2$ (**9h**) is lower than the calculated density of Cu[*t*-BuC(O)CHC(O)*t*-Bu]$_2$, even though the molecular weight of **9h** is higher than that of its non-silylated analogue [16]. We postulated that the lower density for the silylated complex might be an indicator of less efficient packing in the solid-state, which could translate to its observed higher volatility. In the present instances, three new density comparisons can be made concerning the effect of silicon substitution: Cu[MeC(O)CHC(O)SiMe$_3$]$_2$ (**9a**) vs. Cu[MeC(O)CHC(O)*t*-Bu] (**14**) [34], Cu[*i*-PrC(O)CH-

Table 3
Selected bond lengths (Å) and angles (°) for Cu[*i*-PrC(O)CHC(O)SiMe$_3$]$_2$ (**9d**), Cu[*i*-PrC(O)CHC(O)SiMe$_2$(*t*-Bu)]$_2$ (**11d**), Cu[*i*-BuC(O)CHC(O)SiMe$_2$(*t*-Bu)]$_2$ (**11f**), Cu[*s*-BuC(O)CHC(O)SiMe$_2$(*t*-Bu)]$_2$ (**11g**), Cu[*t*-BuC(O)CHC(O)SiMe$_2$(*t*-Bu)]$_2$ (**11h**), and Cu[*t*-BuC(O)CHC(O)Si(*i*-Pr)$_3$]$_2$ (**13h**)

	9d [a]	**11d**/molec 1 [b]	**11d**/molec 2 [b]	**11f** [b]
Bond lengths				
Cu(1)–O(1)	1.919(7)	1.916(8)	1.899(8)	1.911(5)
Cu(1)–O(2)	1.868(7)	1.890(8)	1.876(12)	1.890(5)
Bond angles				
O(1)–Cu(1)–O(2)	92.7(3)	92.9(3)	95.1(4)	93.9(2)
O(1)–Cu(1)–O(2a)	177.7(3)	87.1(3)	84.9(4)	86.1(2)
O(1)–Cu(1)–O(1a)	89.9(4)	180 [c]	180 [c]	180 [c]
O(2)–Cu(1)–O(2a)	84.6(4)	180 [c]	180 [c]	180 [c]

	11g [b]	**11h** [d]	**13h** [b]
Bond lengths			
Cu(1)–O(1)	1.912(6)	1.882(7)	1.906(4)
Cu(1)–O(2)	1.896(5)	1.916(7)	1.895(3)
Bond angles			
O(1)–Cu(1)–O(2)	93.1(2)	93.3(3)	93.1(2)
O(1)–Cu(1)–O(2a)	86.9(2)	177.2(3)	86.9(2)
O(1)–Cu(1)–O(1a)	180 [d]	89.1(4)	180 [d]
O(2)–Cu(1)–O(2a)	180 [d]	84.3(4)	180 [d]

[a] Copper atom is situated on a site of C_{2v} symmetry.
[b] Copper atom is situated on inversion center; there are *two* crystallographically independent *halves* of molecules in the asymmetric unit of **11d**.
[c] Symmetry enforced.
[d] Copper atom is situated on a twofold axis.

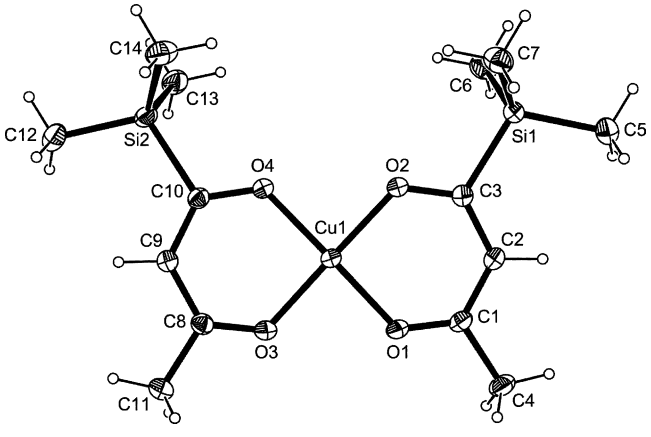

Fig. 3. Molecular structure and atom numbering scheme for Cu[MeC(O)CHC(O)SiMe$_3$]$_2$ (**9a**).

C(O)SiMe$_3$]$_2$ (**9d**) vs. Cu[*i*-PrC(O)CHC(O)*t*-Bu] (**15**) [35], and Cu[*i*-BuC(O)CHC(O)SiMe$_3$]$_2$ (**9f**) vs. Cu[*i*-

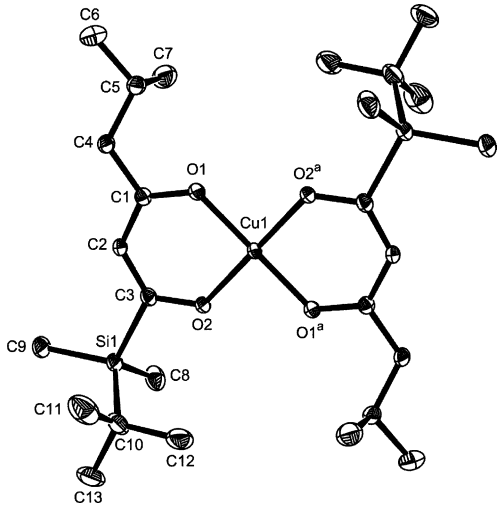

Fig. 4. Molecular structure and atom numbering scheme for Cu[*i*-BuC(O)CHC(O)SiMe$_2$(*t*-Bu)]$_2$ (**11f**). Hydrogen atoms are not shown for clarity.

BuC(O)CHC(O)*t*-Bu]$_2$ (**16**) [27]. However, these comparisons are complicated by the occurrence of different geometrical isomers within each pair of crystals. For the first two pairs, **9a** (*cis*) and **9d** (*cis*) have calculated densities of 1.29 and 1.12 g cm^{-3}, respectively, which are lower than the densities of 1.32 and 1.19 g cm^{-3} reported for the corresponding, non-silylated analogues **14** [34] and **15** [35] (both *trans*). For the third pair of compounds, **9f** (*trans*) and **16** [27] (*cis*) both have essentially the same calculated density of 1.17 g cm^{-3}. Thus once again, the silylated complexes have lower than the expected densities based on molecular weight considerations alone. These observations suggest that the silylated complexes pack in the solid-state differently than the non-silylated complexes, probably due to the longer Si–C bonds contained in two of the peripheral substituents of the ligands.

Interestingly in the instance where we were able to study both geometrical isomers of the same silylated Cu(II) complex Cu[*n*-PrC(O)CHC(O)SiMe$_3$]$_2$ in the solid-state, **9c**-*cis* had a significantly higher density than **9c**-*trans*, viz. 1.20 g cm^{-3} for the former vs. 1.10 g cm^{-3} for the latter. Both complexes crystallized in similar monoclinic unit cells; apparently the *trans*-geometry does not allow for as efficient packing as the more compact *cis*-geometry. Unfortunately, although separate crystals containing different geometrical isomers of **9c** were serendipitously chosen for diffraction studies, they could not be separated for thermal studies.

In a related vein, Cu[*i*-PrC(O)CHC(O)SiMe$_3$]$_2$ (**9d**) (*cis*-geometry in the crystal studied), which is more volatile than Cu[*n*-PrC(O)CHC(O)SiMe$_3$]$_2$ (**9c**) (Table 1), has a density of 1.12 g cm^{-3}, considerably less than that for **9c**-*cis*. While admittedly, the TGA measurements of T_{MWL} were performed on bulk samples that presumably contain a mixture of geometrical isomers,

the density difference likely can be taken again as an indication of less efficient packing, less potential entanglements, and smaller dispersion attractions for the compound with the branched substituent (**9d**), which results in higher volatility.

The present studies illustrate the rich variety of packing motifs in which this class of molecules can crystallize. In order to investigate more quantitatively the differences in packing for Cu(II) β-diketonate complexes, we calculated the solvent-excluded molecular volumes based on the Connolly surfaces for the molecules (Table 4) [37]. The molecular packing density (α) can then be calculated as the product of the Connolly solvent-excluded molecular volume times the number of molecules in the unit cell, divided by the volume of the unit cell, in a method suggested by Troyanov et al. [35], who utilized approximate molecular volumes based on van der Waals radii. The α values based on the Connolly surfaces are generally clustered near an efficiency of ca. 0.580–0.590 with only relatively small variations. However, with due care, some tentative conclusions can be drawn.

We first note that both geometrical isomers of Cu[*n*-PrC(O)CHC(O)SiMe$_3$]$_2$ (**9c**-*cis* and **9c**-*trans*), have the same calculated solvent-excluded molecular volume; however, the packing efficiency is lower for the *trans* complex, due to a larger unit cell volume. Presumably, the molecules with *trans* geometry pack less well than the *cis* molecules. Keeping this observation in mind, we can argue that the complexes Cu[RC(O)CHC(O)SiMe$_3$] pack less efficiently than Cu[RC(O)CHC(O)(*t*-Bu)] (R = Me, *i*-Pr, *i*-Bu, and *t*-Bu). For Cu[*t*-BuC(O)CHC(O)SiMe$_3$]$_2$ (**9h**) and Cu[*t*-BuC(O)CHC(O)*t*-Bu]$_2$ (**17**) [31], where geometrical isomerism is not important, α is ca. 8% lower for the former silylated complex than for the latter. In the cases of Cu[MeC(O)CHC(O)SiMe$_3$] (**9a**) vs. Cu[MeC(O)CHC(O)*t*-Bu] (**14**) and Cu[*i*-Pr(O)CHC(O)SiMe$_3$] (**9d**) vs. Cu[*i*-PrC(O)CHC(O)*t*-Bu] (**15**), the silylated complexes studied had the more efficiently packed *cis* geometry, while the non-silylated analogues were isolated in the roomier *trans* geometry, if we are able to extrapolate from the examples provided by **9c**-*cis* and **9c**-*trans*, above. Here, **9d** still had a significantly lower α value than **15**; for **9a** and **14** one must argue that the similarity in α numbers is due to the different geometrical configurations and that a larger difference would have been observed, if the same geometrical isomers had been studied. Admittedly, a comparison of Cu[*i*-BuC(O)CHC(O)SiMe$_3$] (**9f**) and Cu[*i*-BuRC(O)CHC(O)*t*-Bu] (**16**) seems to fall outside

Table 4
Calculated molecular volumes and packing densities (α) for selected Cu(II) β-diketonate complexes, Cu[R′C(O)CHC(O)R]$_2$

Complex	R′, R	$V_{molecule}$ [a] (Å)^3	Z [b]	$V_{unit\ cell}$ [c] (Å)^3	α [d]
9a	Me, SiMe$_3$	285	2	977	0.583
9b	Et, SiMe$_3$	316	2	1099	0.575
9c-cis	*n*-Pr, SiMe$_3$	352	4	2407	0.585
9c-trans	*n*-Pr, SiMe$_3$	352	4	2609	0.540
9d	*i*-Pr, SiMe$_3$	348	2	1293	0.538
9f	*i*-Bu, SiMe$_3$	386	8	5271	0.586
9h [e]	*t*-Bu, SiMe$_3$	388	4	2749	0.565
10a	Me, SiEt$_3$	384 [f]	4	2613	0.588
11a	Me, SiMe$_2$(*t*-Bu)	392	16	10 907	0.575
11d	*i*-Pr, SiMe$_2$(*t*-Bu)	457 [f]	2	1548	0.590
11f	*i*-Bu, SiMe$_2$(*t*-Bu)	499	1	809	0.617
11g	*s*-Bu, SiMe$_2$(*t*-Bu)	487	2	1632	0.597
11h	*t*-Bu, SiMe$_2$(*t*-Bu)	490	8	6822	0.575
13b	Et, Si(*i*-Pr)$_3$	534	2	1669	0.640
13h	*t*-Bu, Si(*i*-Pr)$_3$	594	2	1931	0.615
14 [g]	Me, *t*-Bu	261	4	1732	0.603
15 [h]	*i*-Pr, *t*-Bu	329	2	1123	0.586
16 [i]	*i*-Bu, *t*-Bu	362	4	2435	0.595
17 [j]	*t*-Bu, *t*-Bu	366	2	1190	0.615

[a] Calculated Connolly solvent-excluded molecular volume.
[b] Number of molecules in the unit cell.
[c] Volume of the unit cell.
[d] Packing density or efficiency, calculated as described in the text.
[e] Ref. [16].
[f] Average molecular volume for the two crystallographically independent molecules.
[g] Ref. [35].
[h] Ref. [36].
[i] Ref. [28].
[j] Ref. [31].

of the above arguments; however, both complexes have disordered peripheral substituents, which makes comparison more problematic.

Within series of silylated complexes, it appears that α values decrease a bit as the size of the non-silylated substituent (R′) increases. However, the variations are relatively small within these series and no definitive conclusions can be reached. Clearly, the factors affecting volatility are manifold, and likely depend in a complex manner on molecular weight, packing pattern, intermolecular and intramolecular contacts and repulsions (including ring stacking and interactions between alkyl side chains), among other properties.

3. Summary

We have demonstrated that the condensation of the lithium enolate of acetyltrialkylsilanes **2a**–**e** with an acyl chloride provides a facile route for the general preparation of the new class of organometalloid-containing ligands, the sila-β-diketones, in good yields. Homoleptic Cu(II) complexes of the new ligands were readily obtained by standard methods. Selective adjustment of the steric demands of the peripheral substituents in the α-trialkylsilyl group or the R′ group at the α′-position of the ligands permits wide attenuation of the physical and thermal properties of the new compounds. For example, most of the complexes containing the $SiEt_3$ substituent were liquids at room temperature, the first such Cu(II) complexes for this class of ligands. Thermal analyses showed that selective incorporation of silicon into the β-diketonate ligands results in enhanced volatility vis-à-vis the corresponding non-silylated, carbon-containing analogues. Single-crystal X-ray diffraction studies suggest that, while silicon substitution has little effect on bonding parameters within the inner coordination sphere and chelate rings of the ligands, the longer Si–C bonds in the SiR_3 groups prevent the complexes from packing efficiently in the solid-state, which may lead to the observed higher volatilities for the silylated complexes. Calculation of molecular packing efficiencies in the solid-state appears to corroborate the latter inference.

The present studies have established the ability to control the volatility and physical state of these novel Cu(II) compounds by variation of the substitution pattern of the metalloid atom in the ligands. Combined with the potential for silicon to scavenge oxygen, these complexes are attractive for CVD applications where contaminations of the films by fluorine and oxygen are of concern.

4. Experimental

4.1. General remarks

All experiments performed under dry dinitrogen utilized standard Schlenk techniques or a Vacuum Atmospheres drybox filled with dinitrogen. Anhydrous diethyl ether and tetrahydrofuran (THF) were distilled from sodium-benzophenone ketyl under a dinitrogen atmosphere prior to use. Hexane was distilled from sodium-benzophenone-diglyme under dinitrogen. Column chromatography was performed using silica gel (40 μm, J.T. Baker).

^{1}H- and ^{13}C-NMR spectra were recorded on a Gemini-300 NMR spectrometer at 300 MHz and 75.43 MHz respectively with $CDCl_3$ as solvent. ^{1}H and ^{13}C chemical shifts are reported relative to the residual signals of the $CDCl_3$ solvent, taken as δ 7.24 for ^{1}H and δ 77.00 for ^{13}C, relative to $SiMe_4$. Electronic spectra were recorded on a Hewlett Packard Diode Array Spectrometer HP8452A in distilled hexane. TGA data were recorded on a TA Instruments TGA 2050 thermogravimetric analyzer under dynamic dry dinitrogen (total flow rate 100 $cm^3\ min^{-1}$), using platinum pans containing a sample size of 1–3 mg, with a ramp rate of 1 °C min^{-1}. DSC measurements were obtained using a TA Instruments DSC 2920 differential scanning calorimeter on 2.0–3.0 mg of sample hermetically sealed in an aluminum pan (dry N_2 flow rate = 8 $cm^3\ min^{-1}$, 1 atm pressure) at a heating rate of 10 °C min^{-1} up to 500 °C and referenced relative to indium. All thermal analyses were calculated using TA Instruments Universal Analysis for Windows 95/98NT version 2.6D. Elemental microanalyses for carbon and hydrogen were determined by MHW Laboratories, Phoenix, AZ.

4.2. General preparation of sila-β-diketones (3–7)

Under dry dinitrogen, a 2 l three-neck flask was charged with anhydrous diethyl ether (250 ml) and diisopropylamine, (11.3 ml, 86.2 mmol). The contents of the flask were cooled to 0 °C, whereupon *n*-BuLi (34.5 ml of a 2.5 M solution in hexane; 86.2 mmol) was added very slowly by syringe to the stirred solution. On completion of the addition, the reaction temperature was maintained at 0 °C for 1 h; the temperature was then lowered to −85 °C and the appropriate acetyltrialkylsilane [23,24] (86.2 mmol) was then added slowly to the mixture. A smooth exothermic reaction followed to form the lithium enolate of the acetyltrialkylsilane. To a second magnetically stirred 1 l single-neck flask, charged with anhydrous ether (250 ml) and the required acyl chloride (86.2 mmol) under dinitrogen and held at −110 °C, was slowly added via cannula the lithium enolate solution while maintaining the reaction temperature between −110 and −75 °C. After 1 h, the

reaction was quenched with saturated aqueous NH_4Cl solution. The organic layer was separated and dried over Na_2SO_4. After the removal of Na_2SO_4 by filtration, the filtrate was concentrated in vacuo. Yields were 40–70%. Further purification of the sila-β-diketonates could be effected via column chromatography using a hexane:-diethyl ether (100:1) eluent according to Still [38]. Elemental analysis data for some of the new compounds and full ^{1}H- and ^{13}C-NMR data follow (ligand **7a** was prepared, but not characterized).

4.2.1. 2,2-Dimethyl-2-silahexane-3,5-dione, *MeC(O)CH$_2$C(O)SiMe$_3$* (**3a**)

Anal. Calc. for $C_7H_{14}O_2Si$: C, 53.12; H, 8.92. Found: C, 53.78; H, 8.49%. ^{1}H-NMR: δ 14.45 (s, 1H, enol O*H*), 5.70 (s, 1H, =C*H*), 2.09 (s, 3H, C*H*$_3$C(O)), 0.17 (s, 9H, Si–C*H*$_3$). ^{13}C-NMR: δ 201.71, 191.61, 109.14, 28.53, −3.22.

4.2.2. 2,2-Dimethyl-2-silaheptane-3,5-dione, *EtC(O)CH$_2$C(O)SiMe$_3$* (**3b**)

Anal. Calc. for $C_8H_{16}O_2Si$: C, 55.77; H, 9.36. Found: C, 55.79; H, 9.40%. ^{1}H-NMR: δ 14.39 (s, 1H, enol O*H*), 5.67 (s, 1H, =C*H*), 2.34 (q, 2H, C*H*$_2$C(O)), 1.07 (t, 3H, CH$_2$C*H*$_3$), 0.15 (s, 9H, Si–C*H*$_3$). ^{13}C-NMR: δ 205.11, 191.10, 108.31, 34.59, 8.59, −3.15.

4.2.3. 2,2-Dimethyl-2-silaoctane-3,5-dione, *n*-*PrC(O)CH$_2$C(O)SiMe$_3$* (**3c**)

Anal. Calc. for $C_9H_{18}O_2Si$: C, 58.02; H, 9.74. Found: C, 58.60; H, 9.62%. ^{1}H-NMR: δ 14.49 (s, 1H, enol O*H*), 5.68 (s, 1H, =C*H*), 2.31 (t, 2H, C*H*$_2$CH$_2$CH$_3$), 1.62 (sext, 2H, CH$_2$C*H*$_2$CH$_3$), 0.93 (t, 3H, CH$_2$CH$_2$C*H*$_3$), 0.18 (s, 9H, Si–C*H*$_3$). ^{13}C-NMR: δ 204.66, 191.51, 108.74, 43.54, 18.33, 13.86, −3.11.

4.2.4. 2,2,6-Trimethyl-2-silaheptane-3,5-dione, *i*-*PrC(O)CH$_2$C(O)SiMe$_3$* (**3d**)

Anal. Calc. for $C_9H_{18}O_2Si$: C, 58.02; H, 9.74. Found: C, 58.61; H, 9.71%. ^{1}H-NMR: δ 14.53 (s, 1H, enol O*H*), 5.71 (s, 1H, =C*H*), 2.50 (sept, 1H, C*H*(CH$_3$)$_2$), 1.09 (d, 6H, CH(C*H*$_3$)$_2$), 0.17 (s, 9H, Si–C*H*$_3$). ^{13}C-NMR: δ 208.27, 192.20, 107.08, 39.41, 18.80, −3.12.

4.2.5. 2,2-Dimethyl-2-silanonane-3,5-dione, *n*-*BuC(O)CH$_2$C(O)SiMe$_3$* (**3e**)

Anal. Calc. for $C_{10}H_{20}O_2Si$: C, 59.95; H, 10.06. Found: C, 60.15; H, 10.34%. ^{1}H-NMR: δ 14.50 (s, 1H, enol O*H*), 5.68 (s, 1H, =C*H*), 2.33 (t, 2H, C*H*$_2$CH$_2$CH$_2$CH$_3$), 1.56 (quint, 2H, CH$_2$C*H*$_2$CH$_2$CH$_3$), 1.32 (sext, 2H, CH$_2$CH$_2$C*H*$_2$CH$_3$), 0.91 (t, 3H, CH$_2$CH$_2$CH$_2$C*H*$_3$), 0.17 (s, 9H, Si–C*H*$_3$). ^{13}C-NMR: δ 204.78, 191.40, 108.72, 41.37, 26.98, 22.47, 13.87, −3.13.

4.2.6. 2,2,7-Trimethyl-2-silaoctane-3,5-dione, *i*-*BuC(O)CH$_2$C(O)SiMe$_3$* (**3f**)

Anal. Calc. for $C_{10}H_{20}O_2Si$: C, 59.95; H, 10.06. Found: C, 60.12; H, 10.28%. ^{1}H-NMR: δ 14.60 (s, 1H, enol O*H*), 5.67 (s, 1H, =C*H*), 2.20 (d, 2H, C*H*$_2$CH), 2.01 (sept, 1H, CH$_2$C*H*), 0.93 (d, 6H, CH(C*H*$_3$)$_2$), 0.18 (s, 9H, Si–C*H*$_3$). ^{13}C-NMR: δ 204.23, 191.60, 109.17, 50.68, 25.70, 22.65, −3.17.

4.2.7. 2,2,6-Trimethyl-2-silaoctane-3,5-dione, *s*-*BuC(O)CH$_2$C(O)SiMe$_3$* (**3g**)

^{1}H-NMR: 14.60 (s, 1H, enol O*H*), 5.67 (s, 1H, =C*H*), 2.27 (sext, 1H, CH$_2$C*H*CH$_3$), 1.60 (m, 1H, C*H*$_2$CH$_3$), 1.36 (m, 1H, C*H*$_2$CH$_3$), 1.04 (d, 3H, CHC*H*$_3$), 0.84 (t, 3H, CH$_2$C*H*$_3$), 0.15 (s, 9H, Si–C*H*$_3$). ^{13}C-NMR: δ 208.06, 192.09, 107.67, 46.65, 26.62, 16.43, 11.69, −3.20.

4.2.8. 2,2,6,6-Tetramethyl-2-silaoctane-3,5-dione, *t*-*BuC(O)CH$_2$C(O)SiMe$_3$* (**3h**)

The analytical data for this compound have been reported previously [16].

4.2.9. 3,3-Diethyl-3-silaheptane-4,6-dione, *MeC(O)CH$_2$C(O)SiEt$_3$* (**4a**)

Anal. Calc. for $C_{10}H_{20}O_2Si$: C, 59.95; H, 10.06. Found: C, 59.72; H, 9.96%. ^{1}H-NMR: δ 14.50 (s, 1H, enol O*H*), 5.67 (s, 1H, =C*H*), 2.09 (s, 3H, C*H*$_3$C(O)), 0.96 (t, 9H, Si–CH$_2$C*H*$_3$), 0.68 (q, 6H, Si–C*H*$_2$CH$_3$). ^{13}C-NMR: δ 201.47, 190.62, 110.55, 28.64, 7.14, 1.96.

4.2.10. 3,3-Diethyl-3-silaoctane-4,6-dione, *EtC(O)CH$_2$C(O)SiEt$_3$* (**4b**)

^{1}H-NMR: δ 14.42 (s, 1H, enol O*H*), 5.65 (s, 1H, =C*H*), 2.35 (q, 2H, CH$_3$C*H*$_2$C(O)), 1.07 (t, 3H, C*H*$_3$CH$_2$C(O)), 0.95 (t, 9H, Si–CH$_2$C*H*$_3$), 0.67 (q, 6H, Si–C*H*$_2$CH$_3$). ^{13}C-NMR: δ 204.68, 189.95, 109.56, 34.53, 8.55, 7.04, 1.92.

4.2.11. 3,3-Diethyl-3-silanonane-4,6-dione, *n*-*PrC(O)CH$_2$C(O)SiEt$_3$* (**4c**)

^{1}H-NMR: δ 14.53 (s, 1H, enol O*H*), 5.66 (s, 1H, =C*H*), 2.31 (t, 2H, C*H*$_2$CH$_2$CH$_3$), 1.62 (sext, 2H, CH$_2$C*H*$_2$CH$_3$), 0.97 (t, 9H, Si–CH$_2$C*H*$_3$), 0.93 (t, 3H, CH$_2$CH$_2$C*H*$_3$), 0.69 (q, 6H, Si–C*H*$_2$CH$_3$). ^{13}C-NMR: δ 202.84, 190.29, 109.99, 43.46, 18.32, 13.73, 7.03, 1.94.

4.2.12. 3,3-Diethyl-7-methyl-3-silaoctane-4,6-dione, *i*-*PrC(O)CH$_2$C(O)SiEt$_3$* (**4d**)

^{1}H-NMR: δ 14.50 (s, 1H, enol O*H*), 5.68 (s, 1H, =C*H*), 2.48 (sept, 1H, C*H*(CH$_3$)$_2$), 1.09 (d, 6H, CH(C*H*$_3$)$_2$), 0.96 (t, 3H, Si–CH$_2$C*H*$_3$), 0.68 (q, 6H, Si–C*H*$_2$CH$_3$). ^{13}C-NMR: δ 207.86, 190.91, 108.37, 39.31, 18.74, 7.04, 1.93.

*4.2.13. 3,3-Diethyl-3-siladecane-4,6-dione, n-BuC(O)CH$_2$C(O)SiEt$_3$ (**4e**)*

^{1}H-NMR: δ 14.52 (s, 1H, enol O*H*), 5.66 (s, 1H, =C*H*), 2.32 (t, 2H, C*H*$_2$CH$_2$CH$_2$CH$_3$), 1.57 (m, 2H, CH$_2$C*H*$_2$CH$_2$CH$_3$), 1.33 (sext, 2H, CH$_2$CH$_2$C*H*$_2$CH$_3$), 0.96 (t, 9H, Si–CH$_2$C*H*$_3$), 0.89 (t, 3H, CH$_2$CH$_2$CH$_2$C*H*$_3$), 0.67 (q, 6H, Si–C*H*$_2$CH$_3$). ^{13}C-NMR: δ 204.28, 190.21, 109.96, 41.27, 26.96, 22.39, 13.76, 7.02, 1.92.

*4.2.14. 3,3-Diethyl-8-methyl-3-silanonane-4,6-dione, i-BuC(O)CH$_2$C(O)SiEt$_3$ (**4f**)*

^{1}H-NMR: δ 14.62 (s, 1H, enol O*H*), 5.65 (s, 1H, =C*H*), 2.19 (d, 2H, C*H*$_2$CH), 2.08 (m, 1H, CH$_2$C*H*), 0.97 (t, 9H, Si–CH$_2$C*H*$_3$), 0.93 (d, 6H, CH(C*H*$_3$)$_2$), 0.68 (q, 6H, Si–C*H*$_2$CH$_3$). ^{13}C-NMR: δ 203.69, 190.61, 110.53, 50.71, 25.84, 22.58, 7.03, 2.02.

*4.2.15. 3,3-Diethyl-7-methyl-3-silanonane-4,6-dione, s-BuC(O)CH$_2$C(O)SiEt$_3$ (**4g**)*

Anal. Calc. for C$_{13}$H$_{26}$O$_2$Si: C, 64.41; H, 10.81. Found: C, 64.22; H, 10.85%. ^{1}H-NMR: δ 14.60 (s, 1H, enol O*H*), 5.67 (s, 1H, =C*H*), 2.29 (sext, 1H, CH$_2$C*H*CH$_3$), 1.63 (m, 1H, C*H*$_2$CH$_3$), 1.40 (m, 1H, C*H*$_2$CH$_3$), 1.08 (d, 3H, CHC*H*$_3$), 0.97 (t, 9H, Si–CH$_2$C*H*$_3$), 0.88 (t, 3H, CHCH$_2$C*H*$_3$), 0.69 (q, 6H, Si–C*H*$_2$CH$_3$). ^{13}C-NMR: δ 207.81, 190.98, 109.12, 46.61, 26.78, 16.49, 11.75, 7.10, 3.00, 1.99.

*4.2.16. 3,3-Diethyl-7,7-dimethyl-3-silaoctane-4,6-dione, t-BuC(O)CH$_2$C(O)SiEt$_3$ (**4h**)*

^{1}H-NMR: δ 14.64 (s, 1H, enol O*H*), 5.83 (s, 1H, =C*H*), 1.12 (s, 9H, C(CH$_3$)$_3$), 0.96 (t, 9H, Si–CH$_2$C*H*$_3$), 0.67 (q, 6H, Si–C*H*$_2$CH$_3$). ^{13}C-NMR: δ 209.55, 191.36, 105.62, 41.65, 26.88, 7.04, 1.97.

*4.2.17. 2,2,3,3-Tetramethyl-3-silaheptane-4,6-dione, MeC(O)CH$_2$C(O)SiMe$_2$(t-Bu) (**5a**)*

^{1}H-NMR: δ 14.47 (s, 1H, enol O*H*), 5.68 (s, 1H, =C*H*), 2.09 (s, 3H, C*H*$_3$C(O)), 0.92 (s, 9H, C(C*H*$_3$)$_3$), 0.12 (s, 6H, Si–C*H*$_3$). ^{13}C-NMR: δ 201.46, 190.93, 110.54, 28.49, 26.33, 7.04, −7.43.

*4.2.18. 2,2,3,3-Tetramethyl-3-silaoctane-4,6-dione, EtC(O)CH$_2$C(O)SiMe$_2$(t-Bu) (**5b**)*

^{1}H-NMR: δ 14.46 (s, 1H, enol O*H*), 5.68 (s, 1H, =C*H*), 2.37 (q, 2H, C*H*$_2$CH$_3$), 1.09 (t, 3H, CH$_2$C*H*$_3$), 0.93 (s, 9H, C(C*H*$_3$)$_3$), 0.12 (s, 6H, Si–C*H*$_3$). ^{13}C-NMR: δ 204.78, 190.31, 109.69, 34.61, 26.38, 16.42, 8.62, −7.34.

*4.2.19. 2,2,3,3-Tetramethyl-3-silanonane-4,6-dione, n-PrC(O)CH$_2$C(O)SiMe$_2$(t-Bu) (**5c**)*

^{1}H-NMR: δ 14.56 (s, 1H, enol O*H*), 5.67 (s, 1H, =C*H*), 2.31 (t, 2H, C*H*$_2$CH$_2$CH$_3$), 1.62 (sext, 2H, CH$_2$C*H*$_2$CH$_3$), 0.93 (s, 9H, C(C*H*$_3$)$_3$), 0.93 (t, 3H, CH$_2$CH$_2$C*H*$_3$), 0.13 (s, 6H, Si–C*H*$_3$). ^{13}C-NMR: δ 204.06, 190.74, 110.09, 43.55, 26.40, 18.39, 16.41, 13.78, −7.35.

*4.2.20. 2,2,3,3,7-Pentamethyl-3-silaoctane-4,6-dione, i-PrC(O)CH$_2$C(O)SiMe$_2$(t-Bu) (**5d**)*

^{1}H-NMR: δ 14.54 (s, 1H, enol O*H*), 5.69 (s, 1H, =C*H*), 2.49 (sept, 1H, C*H*(CH$_3$)$_2$), 1.09 (d, 6H, CH(C*H*$_3$)$_2$), 0.92 (s, 9H, C(C*H*$_3$)$_3$), 0.12 (s, 6H, Si–C*H*$_3$). ^{13}C-NMR: δ 207.86, 191.27, 108.47, 39.35, 26.34, 18.77, 16.36, −7.39.

*4.2.21. 2,2,3,3-Tetramethyl-3-siladecane-4,6-dione, n-BuC(O)CH$_2$C(O)SiMe$_2$(t-Bu) (**5e**)*

^{1}H-NMR: δ 14.55 (s, 1H, enol O*H*), 5.67 (s, 1H, =C*H*), 2.33 (t, 2H, C*H*$_2$CH$_2$CH$_2$CH$_3$), 1.57 (quint, 2H, CH$_2$C*H*$_2$CH$_2$CH$_3$), 1.33 (sext, 2H, CH$_2$CH$_2$C*H*$_2$CH$_3$), 0.93 (s, 9H, C(C*H*$_3$)$_3$), 0.89 (t, 3H, CH$_2$CH$_2$CH$_2$C*H*$_3$), 0.12 (s, 6H, Si–C*H*$_3$). ^{13}C-NMR: δ 204.26, 190.49, 110.04, 41.30, 26.97, 26.34, 22.39, 16.36, 13.79, −7.43.

*4.2.22. 2,2,3,3,8-Pentamethyl-3-silanonane-4,6-dione, i-BuC(O)CH$_2$C(O)SiMe$_2$(t-Bu) (**5f**)*

^{1}H-NMR: δ 14.65 (br, 1H, enol O*H*), 5.65 (s, 1H, =C*H*), 2.19 (d, 2H, C*H*$_2$CH), 2.08 (m, 1H, CH$_2$C*H*), 0.92 (d, 6H, CH(C*H*$_3$)$_2$), 0.92 (s, 9H, C(C*H*$_3$)$_3$), 0.12 (s, 6H, Si–C*H*$_3$). ^{13}C-NMR: δ 203.73, 190.94, 110.62, 50.75, 26.40, 25.86, 22.62, 16.42, −7.37.

*4.2.23. 2,2,3,3,7-Pentamethyl-3-silanonane-4,6-dione, s-BuC(O)CH$_2$C(O)SiMe$_2$(t-Bu) (**5g**)*

^{1}H-NMR: δ 14.64 (s, 1H, enol O*H*), 5.68 (s, 1H, =C*H*), 2.30 (sext, 1H, CH$_2$C*H*CH$_3$), 1.62 (m, 1H, C*H*$_2$CH$_3$), 1.42 (m, 1H, C*H*$_2$CH$_3$), 1.08 (d, 3H, CHC*H*$_3$), 0.93 (s, 9H, C(C*H*$_3$)$_3$), 0.88 (t, 3H, CH$_2$C*H*$_3$), 0.13 (s, 6H, Si–C*H*$_3$). ^{13}C-NMR: δ 207.82, 191.29, 109.20, 46.64, 26.64, 26.38, 16.50, 16.42, 11.76, −7.37.

*4.2.24. 2,2,3,3,7,7-Hexamethyl-3-silaoctane-4,6-dione, t-BuC(O)CH$_2$C(O)SiMe$_2$(t-Bu) (**5h**)*

^{1}H-NMR: δ 14.69 (s, 1H, enol O*H*), 5.85 (s, 1H, =C*H*), 1.12 (s, 9H, (C*H*$_3$)$_3$CC(O)), 0.92 (s, 9H, Si–C(C*H*$_3$)$_3$), 0.12 (s, 6H, Si–C*H*$_3$). ^{13}C-NMR: δ 209.60, 191.69, 105.68, 41.80, 26.90, 26.32, 16.40, −7.41.

*4.2.25. 2,3,3,4,4-Pentamethyl-4-silaoctane-5,7-dione, MeC(O)CH$_2$C(O)SiMe$_2$(t-hexyl) (**6a**)*

^{1}H-NMR: δ 14.62 (br, 1H, enol O*H*), 5.70 (s, 1H, =C*H*), 2.09 (s, 3H, C*H*$_3$C(O)), 1.63 (sept, 1H, SiC(CH$_3$)$_2$C(CH$_3$)$_2$*H*), 0.89 (s, 6H, SiC(C*H*$_3$)$_2$C-(CH$_3$)$_2$H), 0.84 (d, 6H, SiC(CH$_3$)$_2$C(C*H*$_3$)$_2$H), 0.17 (s, 6H, Si–C*H*$_3$). ^{13}C-NMR: δ 209.48, 193.42, 105.57, 41.74, 34.71, 23.82, 20.92, 18.50, −5.00.

*4.2.26. 2,3,3,4,4-Pentamethyl-4-silanonane-5,7-dione, EtC(O)CH$_2$C(O)SiMe$_2$(t-hexyl) (**6b**)*

^{1}H-NMR: δ 14.53 (s, 1H, enol O*H*), 5.67 (s, 1H, =C*H*), 2.33 (q, 2H, C*H*$_2$C(O)), 1.63 (sept, 1H, SiC(CH$_3$)$_2$C(CH$_3$)$_2$*H*), 1.09 (t, 3H, CH$_2$C*H*$_3$), 0.90 (s, 6H, SiC(C*H*$_3$)$_2$C(CH$_3$)$_2$H), 0.85 (d, 6H, SiC(CH$_3$)$_2$C(C*H*$_3$)$_2$H), 0.17 (s, 6H, Si–C*H*$_3$). ^{13}C-NMR: δ 204.53, 191.98, 109.33, 43.65, 34.48, 23.79, 20.85, 18.44, 8.56, −5.07.

*4.2.27. 2,3,3,4,4-Pentamethyl-4-siladecane-5,7-dione, n-PrC(O)CH$_2$C(O)SiMe$_2$(t-hexyl) (**6c**)*

^{1}H-NMR: δ 14.65 (s, 1H, enol O*H*), 5.68 (s, 1H, =C*H*), 2.28 (t, 2H, C*H*$_2$CH$_2$CH$_3$), 1.60 (complex, 3H, SiC(CH$_3$)$_2$C(CH$_3$)$_2$*H* and CH$_2$C*H*$_2$CH$_3$), 0.90 (t, 3H, CH$_2$CH$_2$C*H*$_3$), 0.89 (s, 6H, SiC(C*H*$_3$)$_2$C(CH$_3$)$_2$H), 0.83 (d, 6H, SiC(CH$_3$)$_2$C(C*H*$_3$)$_2$H), 0.15 (s, 6H, Si–C*H*$_3$). ^{13}C-NMR: δ 204.01, 192.33, 109.78, 43.43, 34.68, 23.81, 20.86, 18.45, 18.35, 13.73, −5.09.

*4.2.28. 2,3,3,4,4,8-Hexamethyl-4-silanonane-5,7-dione, i-PrC(O)CH$_2$C(O)SiMe$_2$(t-hexyl) (**6d**)*

^{1}H-NMR: δ 14.59 (s, 1H, enol O*H*), 5.71 (s, 1H, =C*H*), 2.49 (sept, 1H, C*H*(CH$_3$)$_2$), 1.62 (sept, 1H, SiC(CH$_3$)$_2$C(CH$_3$)$_2$*H*), 1.09 (d, 6H, CH(C*H*$_3$)$_2$), 0.89 (s, 6H, SiC(C*H*$_3$)$_2$C(CH$_3$)$_2$H), 0.84 (d, 6H, SiC(CH$_3$)$_2$C(C*H*$_3$)$_2$H), 0.17 (s, 6H, Si–C*H*$_3$). ^{13}C-NMR: δ 207.84, 193.08, 108.24, 39.34, 34.68, 23.81, 20.88, 18.79, 18.47, −5.04.

*4.2.29. 2,3,3,4,4-Pentamethyl-4-silaundecane-5,7-dione, n-BuC(O)CH$_2$C(O)SiMe$_2$(t-hexyl) (**6e**)*

^{1}H-NMR: δ 14.63 (s, 1H, enol O*H*), 5.69 (s, 1H, =C*H*), 2.33 (t, 2H, C*H*$_2$CH$_2$CH$_2$CH$_3$), 1.63 (sept, 1H, SiC(CH$_3$)$_2$C(CH$_3$)$_2$*H*), 1.57 (quint, 2H, CH$_2$C*H*$_2$CH$_2$CH$_3$), 1.33 (sext, 2H, CH$_2$CH$_2$C*H*$_2$CH$_3$), 0.91 (s, 6H, SiC(C*H*$_3$)$_2$C(CH$_3$)$_2$H), 0.90 (t, 3H, CH$_2$CH$_2$CH$_2$C*H*$_3$), 0.85 (d, 6H, SiC(CH$_3$)$_2$C(C*H*$_3$)$_2$H), 0.17 (s, 6H, Si–C*H*$_3$). ^{13}C-NMR: δ 204.08, 192.44, 109.79, 41.28, 34.77, 27.08, 23.91, 22.41, 20.94, 18.50, 13.75, −5.01.

*4.2.30. 2,3,3,4,4,9-Hexamethyl-4-siladecane-5,7-dione, i-BuC(O)CH$_2$C(O)SiMe$_2$(t-hexyl) (**6f**)*

^{1}H-NMR: δ 14.74 (s, 1H, enol O*H*), 5.67 (s, 1H, =C*H*), 2.19 (d, 2H, C*H*$_2$CH), 2.07 (m, 1H, CH$_2$C*H*), 1.62 (sept, 1H, SiC(CH$_3$)$_2$C(CH$_3$)$_2$*H*), 0.92 (d, 6H, CH(C*H*$_3$)$_2$), 0.90 (s, 6H, SiC(C*H*$_3$)$_2$C(CH$_3$)$_2$H), 0.84 (d, 6H, SiC(CH$_3$)$_2$C(C*H*$_3$)$_2$H), 0.16 (s, 6H, Si–C*H*$_3$). ^{13}C-NMR: δ 203.72, 192.65, 110.34, 50.67, 34.71, 25.92, 23.86, 22.58, 20.90, 18.47, −5.09.

*4.2.31. 2,3,3,4,4,8-Hexamethyl-4-siladecane-5,7-dione, s-BuC(O)CH$_2$C(O)SiMe$_2$(t-hexyl) (**6g**)*

^{1}H-NMR: δ 14.72 (s, 1H, enol O*H*), 5.71 (s, 1H, =C*H*), 2.29 (sext, 1H, CH$_2$C*H*CH$_3$), 1.63 (complex, 2H, SiC(CH$_3$)$_2$C(CH$_3$)$_2$*H* and C*H*$_2$CH$_3$), 1.40 (m, 1H, C*H*$_2$CH$_3$), 1.07 (d, 3H, CHC*H*$_3$), 0.91 (s, 6H, SiC(C*H*$_3$)$_2$C(CH$_3$)$_2$H), 0.87 (t, 3H, CH$_2$C*H*$_3$), 0.85 (d, 6H, SiC(CH$_3$)$_2$C(C*H*$_3$)$_2$H), 0.18 (s, 6H, Si–C*H*$_3$). ^{13}C-NMR: δ 207.70, 193.07, 108.96, 46.61, 34.73, 28.82, 23.87, 20.93, 18.50, 16.50, 11.74, −5.03.

*4.2.32. 2,3,3,4,4,8,8-Heptamethyl-4-silanonane-5,7-dione, t-BuC(O)CH$_2$C(O)SiMe$_2$(t-hexyl) (**6h**)*

^{1}H-NMR: δ 14.77 (s, 1H, enol O*H*), 5.88 (s, 1H, =C*H*), 1.62 (sept, 1H, SiC(CH$_3$)$_2$C(CH$_3$)$_2$*H*), 1.24 (s, 9H, C(C*H*$_3$)$_3$), 0.89 (s, 6H, SiC(C*H*$_3$)$_2$C(CH$_3$)$_2$H), 0.84 (d, 6H, SiC(CH$_3$)$_2$C(C*H*$_3$)$_2$H), 0.17 (s, 6H, Si–C*H*$_3$). ^{13}C-NMR: δ 209.48, 193.42, 105.57, 41.74, 34.71, 26.95, 23.82, 20.92, 18.50, −5.00.

*4.2.33. 3,3-Diisopropyl-2-methyl-3-silaoctane-4,6-dione, EtC(O)CH$_2$C(O)Si(i-Pr)$_3$ (**7b**)*

^{1}H-NMR: δ 14.58 (s, 1H, enol O*H*), 5.69 (s, 1H, =C*H*), 2.36 (q, 2H, C*H*$_2$C(O)), 1.19 (m, 3H, Si–C*H*(CH$_3$)$_2$), 1.08 (d, 18H, Si–CH(C*H*$_3$)$_2$), 1.07 (t, 3H, CH$_2$C*H*$_3$). ^{13}C-NMR: δ 204.40, 189.62, 110.60, 34.57, 18.33, 10.68, 10.30.

*4.2.34. 3,3-Diisopropyl-2-methyl-3-silanonane-4,6-dione, n-PrC(O)CH$_2$C(O)Si(i-Pr)$_3$ (**7c**)*

Anal. Calc. for C$_{15}$H$_{30}$O$_2$Si: C, 66.61; H, 11.18. Found: C, 66.00; H, 11.60%. ^{1}H-NMR: δ 14.69 (s, 1H, enol O*H*), 5.69 (s, 1H, =C*H*), 2.31 (t, 2H, C*H*$_2$CH$_2$CH$_3$), 1.62 (sext, 2H, CH$_2$C*H*$_2$CH$_3$), 1.19 (m, 3H, Si–C*H*(CH$_3$)$_2$), 1.01 (d, 18H, Si–CH(C*H*$_3$)$_2$), 0.93 (t, 3H, CH$_2$CH$_2$C*H*$_3$). ^{13}C-NMR: δ 203.79, 189.99, 111.04, 43.49, 18.46, 18.32, 13.73, 10.31.

*4.2.35. 3,3-Diisopropyl-2,7-dimethyl-4-silaoctane-4,6-dione, i-PrC(O)CH$_2$C(O)Si(i-Pr)$_3$ (**7d**)*

^{1}H-NMR: δ 14.62 (s, 1H, enol O*H*), 5.9 (s, 1H, =C*H*), 2.49 (sept, 1H, C(O)C*H*(CH$_3$)$_2$), 1.07 (d, 6H, C(O)CH(C*H*$_3$)$_2$), 1.06 (d, 18H, Si–CH(C*H*$_3$)$_2$), 1.02 (m, 3H, Si–C*H*(CH$_3$)$_2$). ^{13}C-NMR: δ 207.39, 190.32, 109.43, 39.27, 18.72, 18.27, 10.26.

*4.2.36. 3,3-Diisopropyl-2-methyl-4-siladecane-4,6-dione, n-BuC(O)CH$_2$C(O)Si(i-Pr)$_3$ (**7e**)*

Anal. Calc. for C$_{16}$H$_{32}$O$_2$Si: C, 67.55; H, 11.34. Found: C, 67.27; H, 11.76%. ^{1}H-NMR: δ 14.70 (s, 1H, enol O*H*), 5.71 (s, 1H, =C*H*), 2.34 (t, 2H, C*H*$_2$CH$_2$CH$_2$CH$_3$), 1.59 (quint, 2H, CH$_2$C*H*$_2$CH$_2$CH$_3$), 1.34 (m, 2H, CH$_2$CH$_2$C*H*$_2$CH$_3$), 1.21 (m, 3H, Si–C*H*(CH$_3$)$_2$), 1.10 (d, 18H, Si–CH(C*H*$_3$)$_2$), 0.91 (t, 3H, CH$_2$CH$_2$CH$_2$C*H*$_3$). ^{13}C-NMR: δ 204.12, 190.03, 111.11, 41.39, 27.16, 22.44, 18.39, 13.64, 10.35.

4.2.37. 3,3-Diisopropyl-2,8-dimethyl-3-silanonane-4,6-dione, i-BuC(O)CH$_2$C(O)Si(i-Pr)$_3$ (7f)

^{1}H-NMR: δ 14.80 (s, 1H, enol OH), 5.68 (s, 1H, =CH), 2.19 (d, 2H, CH$_2$CH), 2.10 (m, 1H, CH$_2$CH), 1.20 (m, 3H, Si–CH(CH$_3$)$_2$), 1.09 (d, 18H, Si–CH(CH$_3$)$_2$), 0.93 (d, 6H, CH(CH$_3$)$_2$). ^{13}C-NMR: δ 203.58, 190.39, 111.69, 50.77, 26.11, 22.64, 18.39, 10.36.

4.2.38. 3,3-Diisopropyl-2,7-dimethyl-3-silanonane-4,6-dione, s-BuC(O)CH$_2$C(O)Si(i-Pr)$_3$ (7g)

^{1}H-NMR: δ 14.73 (s, 1H, enol OH), 5.70 (s, 1H, =CH), 2.28 (sext, 1H, CH$_2$CHCH$_3$), 1.62 (m, 1H, CH$_2$CH$_3$), 1.41 (m, 1H, CH$_2$CH$_3$), 1.20 (m, 3H, Si–CH(CH$_3$)$_2$), 1.09 (d, 18H, Si–CH(CH$_3$)$_2$), 1.06 (d, 3H, CHCH$_3$), 0.88 (t, 3H, CH$_2$CH$_3$). ^{13}C-NMR: δ 207.25, 190.70, 110.16, 46.62, 26.89, 18.37, 16.47, 11.65, 10.41.

4.2.39. 3,3-Diisopropyl-2,7,7-trimethyl-4-silaoctane-4,6-dione, t-BuC(O)CH$_2$C(O)Si(i-Pr)$_3$ (7h)

Anal. Calc. for C$_{16}$H$_{32}$O$_2$Si: C, 67.55; H, 11.34. Found: C, 67.39; H, 11.26%. ^{1}H-NMR: δ 14.70 (s, 1H, enol OH), 5.87 (s, 1H, =CH), 1.18 (sept, 3H, Si–CH(CH$_3$)$_2$), 1.13 (s, 9H, C(CH$_3$)$_3$), 1.08 (d, 18H, Si–CH(CH$_3$)$_2$). ^{13}C-NMR: δ 209.29, 190.73, 107.01, 41.65, 18.47, 18.35, 10.32.

4.3. Synthesis of sila-β-diketonate copper(II) complexes, Cu[R′C(O)CHC(O)SiR$_3$]$_2$

The homoleptic copper(II) sila-β-diketonate complexes could be readily prepared by any of the three following methods. Methods (a) and (b) provide somewhat higher yields (> 80% based on diketone); however, method (c) gives the desired complexes under somewhat milder conditions. Further, method (c) can be applied to unpurified sila-β-diketones, in what is tantamount to a one-step procedure. Yields are somewhat variable for the latter method (40–80%), but purification of the ligand is not required, the exclusion of air and water is not necessary.

4.3.1. Method (a): formation of Cu(II) complexes under aprotic conditions

To a stirred solution of purified sila-β-diketone (1.3 mmol) dissolved in dry THF (100 ml) under dinitrogen was slowly added potassium hydride (0.05 g, 1 mmol). The mixture was allowed to react for 30 min, after which unreacted KH was removed by filtration. The filtrate was slowly reacted with copper(II) chloride dihydrate (0.11 g, 6.3 mmol), which resulted in the formation of a deep green solution. The solvent was removed in vacuo, providing the crude copper(II) compound, which was purified by either sublimation or recrystallization from diethyl ether to afford the analytically pure metal complex.

4.3.2. Method (b): formation of Cu(II) complexes under protic conditions

The sila-β-diketone (1.3 mmol) was dissolved in 95% ethanol (80 ml). To the stirred solution, a solution of sodium hydroxide (0.1 g, 3 mmol) in 95% ethanol (10 ml) was slowly added and allowed to react for 15 min. Copper(II) chloride dihydrate (0.11 g, 6.3 mmol) was then added which resulted in the formation of a deep green solution. The solvent was removed in vacuo to provide the crude copper(II) complex, which was purified as in method (a) (Section 4.3.1).

4.3.3. Method (c): direct formation of Cu(II) complexes using purified sila-β-diketones

To a vigorously stirred solution of copper(II) acetate hydrate (3.00 g, 15 mmol) in water (100 ml), a solution of sila-β-diketone (25 mmol) dissolved in diethyl ether (100 ml) was added. The organic layer immediately turned deep green and stirring was continued for 1 h. The diethyl ether was removed in vacuo. Extraction of the remaining reaction mixture with hexane, followed by separation, drying over Na_2SO_4, and concentration of the organic layer resulted in the isolation of the crude copper(II) complex. If pure sila-β-diketone was utilized, the green product was generally obtained as a solid; on the other hand, use of unpurified ligand led to the isolation of a green oil. In either case, column chromatography on silica gel using a 100:1 hexane–ether eluent system provided the purification of the crude copper(II) complex. Further purification could be effected as in method (a) (Section 4.3.1).

4.3.4. Elemental analyses for the new complexes

Cu[MeC(O)CHC(O)SiMe$_3$]$_2$ (**9a**). Anal. Calc. for C$_{14}$H$_{26}$CuO$_4$Si$_2$: C, 44.48; H, 6.93. Found: C, 44.56; H, 6.81%; Cu[EtC(O)CHC(O)SiMe$_3$]$_2$ (**9b**). Anal. Calc. for C$_{16}$H$_{30}$CuO$_4$Si$_2$: C, 47.32; H, 7.45. Found: C, 47.31; H, 7.42%; Cu[*n*-PrC(O)CHC(O)SiMe$_3$]$_2$ (**9c**). Anal. Calc. for C$_{18}$H$_{34}$CuO$_4$Si$_2$: C, 49.79; H, 7.89. Found: C, 50.02; H, 8.02%; Cu[*i*-PrC(O)CHC(O)SiMe$_3$]$_2$ (**9d**). Anal. Calc. for C$_{18}$H$_{34}$CuO$_4$Si$_2$: C, 49.79; H, 7.89. Found: C, 50.03; H, 7.67%; Cu[*n*-BuC(O)CHC(O)SiMe$_3$]$_2$ (**9e**). Anal. Calc. for C$_{20}$H$_{38}$CuO$_4$Si$_2$: C, 51.97; H, 8.29. Found: C, 52.18; H, 8.25%; Cu[*i*-BuC(O)CHC(O)SiMe$_3$]$_2$ (**9f**). Anal. Calc. for C$_{20}$H$_{38}$CuO$_4$Si$_2$: C, 51.97; H, 8.29. Found: C, 51.76; H, 8.04%; Cu[*s*-BuC(O)CHC(O)SiMe$_3$]$_2$ (**9g**). Anal. Calc. for C$_{20}$H$_{38}$CuO$_4$Si$_2$: C, 51.97; H, 8.29. Found: C, 52.05; H, 8.02%; Cu[*t*-BuC(O)CHC(O)SiMe$_3$]$_2$ (**9h**). Anal. Calc. for C$_{20}$H$_{38}$CuO$_4$Si$_2$: C, 51.97; H, 8.29. Found: C, 52.12; H, 8.23%; Cu[MeC(O)CHC(O)SiEt$_3$]$_2$ (**10a**). Anal. Calc. for C$_{20}$H$_{38}$CuO$_4$Si$_2$: C, 51.97; H, 8.29. Found: C, 51.76; H, 8.09%; Cu[EtC(O)CHC(O)SiEt$_3$]$_2$ (**10b**). Anal. Calc. for C$_{22}$H$_{42}$CuO$_4$Si$_2$: C, 53.90; H, 8.63. Found: C, 54.30; H, 8.47%; Cu[*n*-PrC(O)CHC(O)SiEt$_3$]$_2$ (**10c**). Anal. Calc. for C$_{24}$H$_{46}$CuO$_4$Si$_2$: C,

55.61; H, 8.95. Found: C, 55.49; H, 8.82%; Cu[*i*-PrC(O)CHC(O)SiEt$_3$]$_2$ (**10d**). Anal. Calc. for $C_{24}H_{46}CuO_4Si_2$: C, 55.61; H, 8.95. Found: C, 55.46; H, 8.80%; Cu[*n*-BuC(O)CHC(O)SiEt$_3$]$_2$ (**10e**). Anal. Calc. for $C_{26}H_{50}CuO_4Si_2$: C, 57.15; H, 9.22. Found: C, 51.03; H, 7.86%; Cu[*i*-BuC(O)CHC(O)SiEt$_3$]$_2$ (**10f**). Anal. Calc. for $C_{26}H_{50}CuO_4Si_2$: C, 57.15; H, 9.22. Found: C, 57.36; H, 9.14%; Cu[*s*-BuC(O)CHC(O)SiEt$_3$]$_2$ (**10g**). Anal. Calc. for $C_{26}H_{50}CuO_4Si_2$: C, 57.15; H, 9.22. Found: C, 57.36; H, 9.14%; Cu[*t*-BuC(O)CHC(O)SiEt$_3$]$_2$ (**10h**). Anal. Calc. for $C_{26}H_{50}CuO_4Si_2$: C, 57.15; H, 9.22. Found: C, 57.07; H, 9.12%; Cu[MeC(O)CHC(O)SiMe$_2$(*t*-Bu)]$_2$ (**11a**). Anal. Calc. for $C_{20}H_{38}CuO_4Si_2$: C, 51.97; H, 8.29. Found: C, 51.76; H, 8.06%; Cu[EtC(O)CHC(O)SiMe$_2$(*t*-Bu)]$_2$ (**11b**). Anal. Calc. for $C_{22}H_{42}CuO_4Si_2$: C, 53.90; H, 8.63. Found: C, 53.70; H, 8.50%; Cu[*n*-PrC(O)CHC(O)SiMe$_2$(*t*-Bu)]$_2$ (**11c**). Anal. Calc. for $C_{24}H_{46}CuO_4Si_2$: C, 55.61; H, 8.95. Found: C, 55.81; H, 8.70%; Cu[*i*-PrC(O)CHC(O)SiMe$_2$(*t*-Bu)]$_2$ (**11d**). Anal. Calc. for $C_{24}H_{46}CuO_4Si_2$: C, 55.61; H, 8.95. Found: C, 55.56; H, 8.87%; Cu[*n*-BuC(O)CHC(O)SiMe$_2$(*t*-Bu)]$_2$ (**11e**). Anal. Calc. for $C_{26}H_{50}CuO_4Si_2$: C, 57.15; H, 9.22. Found: C, 57.11; H, 9.02%; Cu[*i*-BuC(O)CHC(O)SiMe$_2$(*t*-Bu)]$_2$ (**11f**). Anal. Calc. for $C_{26}H_{50}CuO_4Si_2$: C, 57.15; H, 9.22. Found: C, 57.26; H, 9.10%; Cu[*s*-BuC(O)CHC(O)SiMe$_2$(*t*-Bu)]$_2$ (**11g**). Anal. Calc. for $C_{26}H_{50}CuO_4Si_2$: C, 57.15; H, 9.22. Found: C, 57.03; H, 9.11%; Cu[*t*-BuC(O)CHC(O)SiMe$_2$(*t*-Bu)]$_2$ (**11h**). Anal. Calc. for $C_{26}H_{50}CuO_4Si_2$: C, 57.15; H, 9.22. Found: C, 57.02; H, 9.39%; Cu[MeC(O)CHC(O)SiMe$_2$(*t*-hexyl)]$_2$ (**12a**). Anal. Calc. for $C_{24}H_{46}CuO_4Si_2$: C, 55.61; H, 8.95. Found: C, 55.54; H, 8.86%; Cu[EtC(O)CHC(O)SiMe$_2$(*t*-hexyl)]$_2$ (**12b**). Anal. Calc. for $C_{26}H_{50}CuO_4Si_2$: C, 57.15; H, 9.22. Found: C, 57.04; H, 9.02%; Cu[*n*-PrC(O)CHC(O)SiMe$_2$(*t*-hexyl)]$_2$ (**12c**). Anal. Calc. for $C_{28}H_{54}CuO_4Si_2$: C, 58.54; H, 9.48. Found: C, 58.59; H, 9.37%; Cu[*i*-PrC(O)CHC(O)SiMe$_2$(*t*-hexyl)]$_2$ (**12d**). Anal. Calc. for $C_{28}H_{54}CuO_4Si_2$: C, 58.54; H, 9.48. Found: C, 58.70; H, 9.52%; Cu[*n*-BuC(O)CHC(O)SiMe$_2$(*t*-hexyl)]$_2$ (**12e**). Anal. Calc. for $C_{30}H_{58}CuO_4Si_2$: C, 59.81; H, 9.70. Found: C, 60.05; H, 9.57%; Cu[*i*-BuC(O)CHC(O)SiMe$_2$(*t*-hexyl)]$_2$ (**12f**). Anal. Calc. for $C_{30}H_{58}CuO_4Si_2$: C, 59.81; H, 9.70. Found: C, 60.01; H, 9.52%; Cu[*s*-BuC(O)CHC(O)SiMe$_2$(*t*-hexyl)]$_2$ (**12g**). Anal. Calc. for $C_{30}H_{58}CuO_4Si_2$: C, 59.81; H, 9.70. Found: C, 60.07; H, 9.96%; Cu[*t*-BuC(O)CHC(O)SiMe$_2$(*t*-hexyl)]$_2$ (**12h**). Anal. Calc. for $C_{30}H_{58}CuO_4Si_2$: C, 59.81; H, 9.70. Found: C, 59.69; H, 9.66%; Cu[EtC(O)CHC(O)Si(*i*-Pr)$_3$]$_2$ (**13b**). Anal. Calc. for $C_{28}H_{54}CuO_4Si_2$: C, 58.54; H, 9.48. Found: C, 58.62; H, 9.29%; Cu[*n*-PrC(O)CHC(O)Si(*i*-Pr)$_3$]$_2$ (**13c**). Anal. Calc. for $C_{30}H_{58}CuO_4Si_2$: C, 59.81; H, 9.70. Found: C, 61.09; H, 8.40%; Cu[*i*-PrC(O)CHC(O)Si(*i*-Pr)$_3$]$_2$ (**13d**). Anal. Calc. for $C_{28}H_{54}CuO_4Si_2$: C, 59.81; H, 9.70. Found: C, 59.95; H, 9.51%; Cu[*n*-BuC(O)CHC(O)Si(*i*-Pr)$_3$]$_2$ (**13e**). Anal. Calc. for $C_{32}H_{62}CuO_4Si_2$: C, 60.95; H, 9.91. Found: C, 59.21; H, 10.40%; Cu[*i*-BuC(O)CHC(O)Si(*i*-Pr)$_3$]$_2$ (**13f**). Anal. Calc. for $C_{32}H_{62}CuO_4Si_2$: C, 60.95; H, 9.91. Found: C, 60.78; H, 9.96%; Cu[*s*-BuC(O)CHC(O)Si(*i*-Pr)$_3$]$_2$ (**13g**). Anal. Calc. for $C_{32}H_{62}CuO_4Si_2$: C, 60.95; H, 9.91. Found: C, 60.85; H, 9.75.

4.4. Calculation of Connolly solvent-excluded molecular volumes

All Connolly solvent-excluded molecular volumes were calculated via the program, CAMBRIDGESOFT CHEM3D ULTRA Version 7.0.0, using a Dell Dimension 4500 Pentium® 4 CPU (2.40 GHz) with 1.00 GB RAM running under Windows XP Professional. The Connolly solvent-excluded molecular volume is defined as the volume enclosed within the contact surface created by rolling a spherical probe over the molecular model [37]. The Connolly molecular surface (contact surface) represents the solvent-accessible surface.

Coordinates for the molecular models were taken from the corresponding coordinates determined by single-crystal X-ray diffraction studies. Several spherical probe sizes were tried in the calculations, ranging from a diameter of 0.010–2.0 Å; while variation of the probe size naturally changed the calculated solvent-excluded volume, the relative sizes of the molecular volumes did not change appreciably with respect to one another. Thus, we chose to use the default diameter of 1.4 Å for the spherical probe (approximately the size of a water molecule).

4.5. X-ray structure determinations

Crystals suitable for X-ray diffraction studies were obtained by slow evaporation of saturated solutions of the desired compound at room temperature. All compounds studied were very soluble; pentane, ethanol, ethanol/water, acetone/water or diethyl ether solutions provided suitable crystals. In no cases were solvent molecules found definitively to coordinate to copper or to form solvates, except possibly for the copper complexes with SiEt$_3$-substituted ligands (see Section 2).

Unit cell parameters were determined from 20 to 25 well-centered, intense reflections in the range $15^\circ \leq 2\theta \leq 25^\circ$. A Siemens (Bruker) R3m diffractometer in the $\omega/2\theta$ mode (except for **9a** and **9d**, $\theta/2\theta$ mode), with variable scan speed (3–20° min^{-1}) and graphite monochromated Mo–K$_\alpha$ radiation ($\lambda = 0.71073$ Å), was used to collect the intensity data at ambient temperature. For crystals of each compound, data were corrected for background, attenuators, and Lorentz and polarization effects in the usual fashion [39]. Semi-empirical absorption corrections were applied to **9a**, **9b**, **9c**-*cis*, **9f**, **11d**, **11f**, **11h**, **13b**, and **13h** using the ψ-scan method.

Table 5
Crystallographic data and parameters for **8** and the Cu(II) complexes

	8	**9a**	**9b**	**9c**-*cis*	**9c**-trans	**9d**	**9f**	**10a**	**11a**	**11d**	**11f**	**11g**	**11h**	**13b**	**13h**
Formula	$C_{15}H_{34}O_3Si_2$	$C_{14}H_{26}CuO_4Si_2$	$C_{16}H_{30}CuO_4Si_2$	$C_{18}H_{34}CuO_4Si_2$	$C_{18}H_{34}CuO_4Si_2$	$C_{18}H_{34}CuO_4Si_2$	$C_{20}H_{38}CuO_4Si_2$	$C_{20}H_{38}CuO_4Si_2$	$C_{20}H_{38}CuO_4Si_2$	$C_{24}H_{46}CuO_4Si_2$	$C_{26}H_{50}CuO_4Si_2$	$C_{26}H_{50}CuO_4Si_2$	$C_{26}H_{50}CuO_4Si_2$	$C_{28}H_{54}CuO_4Si_2$	$C_{32}H_{62}CuO_4Si_2$
Formula weight	318.6	378.1	406.1	434.2	434.2	434.2	462.2	462.2	462.2	518.3	546.4	546.4	546.4	574.4	630.5
Crystal color; habit	Colorless needle	Dark green plate	Dark green block	Dark green-black prism	Green prism	Dark green-brown plate	Dark green parallelepiped	Olive green prism	Black prism	Dark green parallelepiped	Dark green prism	Green-black prism	Dark green prism	Blue-green prism	Olive plate
Crystal dimensions (mm)	0.35 × 0.35 × 0.80	0.20 × 0.60 × 0.90	0.25 × 0.55 × 0.65	0.30 × 0.35 × 0.95	0.25 × 0.25 × 0.50	0.10 × 0.30 × 0.50	0.40 × 0.50 × 0.70	0.30 × 0.30 × 0.40	0.50 × 0.60 × 0.80	0.30 × 0.40 × 0.50	0.10 × 0.30 × 0.40	0.20 × 0.30 × 0.40	0.35 × 0.40 × 0.70	0.15 × 0.40 × 0.60	0.20 × 0.50 × 0.75
Crystal system	Orthorhombic	Triclinic	Triclinic	Monoclinic	Monoclinic	Tetragonal	Monoclinic	Triclinic	Tetragonal	Triclinic	Triclinic	Monoclinic	Orthorhombic	Triclinic	Monoclinic
Space group	$P2_12_12_1$ (No. 19)	$P\bar{1}$ (No. 2)	$P\bar{1}$ (No. 2)	$P2_1/n$ (No. 14)	$P2_1/n$ (No. 14)	$P\bar{4}2_1m$ (No. 113)	$C2/c$ (No. 15)	$P\bar{1}$ (No. 2)	$I4_1/a$ (No. 88)	$P\bar{1}$ (No. 2)	$P\bar{1}$ (No. 2)	$P2_1/n$ (No. 14)	$Fdd2$ (No. 43)	$P\bar{1}$ (No. 2)	$P2_1/c$ (No. 14)
a (Å)	9.776(3)	9.618(2)	10.159(3)	13.093(2)	14.162(7)	9.952(2)	25.482(11)	12.944(6)	27.551(7)	11.181(4)	6.807(2)	10.777(2)	22.814(8)	8.573(1)	14.244(5)
b (Å)	12.326(4)	9.822(2)	10.723(4)	9.844(2)	9.813(8)	9.952(2)	10.128(3)	14.079(5)	27.551(7)	12.445(4)	10.529(3)	12.869(3)	24.877(9)	14.562(2)	11.593(4)
c (Å)	16.589(8)	10.573(2)	11.100(3)	19.234(5)	19.303(12)	13.057(3)	21.136(8)	16.068(6)	14.369(5)	12.682(4)	11.418(3)	11.853(2)	12.021(3)	14.997(3)	11.772(4)
α (°)	90	82.68(2)	70.76(2)	90	90	90	90	66.71(3)	90	62.72(2)	89.12(2)	90	90	109.70(1)	90
β (°)	90	80.40(2)	74.32(3)	103.84(2)	103.46(5)	90	104.93(3)	76.97(3)	90	80.71(3)	86.14(2)	97.04(1)	90	97.15(1)	96.64(3)
γ (°)	90	89.63(2)	82.98(3)	90	90	90	90	88.85(3)	90	85.03(3)	82.14(2)	90	90	103.72(1)	90
V (Å^3)	1999.0(13)	976.7(4)	1098.6(6)	2407.1(10)	2609(3)	1293.1(5)	5271(4)	2613(2)	10907(7)	1547.5(9)	808.7(4)	1631.6(6)	6822(4)	1669.0(5)	1930.7(12)
Z	4	2	2	4	4	2	8	4	16	2	1	2	8	2	2
D_{calc} (g cm^{-3})	1.059	1.286	1.228	1.198	1.105	1.115	1.165	1.175	1.126	1.112	1.122	1.112	1.064	1.198	1.085
μ(Mo–K$_\alpha$) (cm^{-1})	1.82	12.51	11.17	10.23	9.44	9.52	9.39	9.47	9.07	8.06	7.74	7.67	7.34	10.23	6.56
F(0 0 0)	704	398	430	924	924	462	1976	988	3952	558	295	590	2360	924	686
2θ max (°)	45.0	55.0	48.0	45.0	45.0	45.0	45.0	45.0	45.0	45.0	45.0	45.0	50.0	48.0	45.0
Reflections collected	1521	4414	3665	3241	3481	1005	3531	6971	3731	3957	2255	2266	1589	5451	2633
Independent reflections	1521 [R_{int} = 0.00%]	4200 [R_{int} = 3.66%]	3461 [R_{int} = 4.66%]	3132 [R_{int} = 3.18%]	3367 [R_{int} = 5.45%]	553 [R_{int} = 2.19%]	3414 [R_{int} = 3.91%]	6626 [R_{int} = 0.97%]	3549 [R_{int} = 2.54%]	3742 [R_{int} = 3.31%]	2125 [R_{int} = 2.54%]	2125 [R_{int} = 1.18%]	1589 [R_{int} = 0.00%]	5224 [R_{int} = 2.25%]	2516 [R_{int} = 3.88%]
Observed reflections	1164 ($F >$ 4.0σ(F))	3351 ($F >$ 6.0σ(F))	2202 ($F >$ 6.0σ(F))	2104 ($F >$ 4.0σ(F))	1824 ($F >$ 4.0σ(F))	389 ($F >$ 4.0σ(F))	2209 ($F >$ 4.0σ(F))	2001 ($F >$ 4.0σ(F))	2545 ($F >$ 4.0σ(F))	1899 ($F >$ 6.0σ(F))	1283 ($F >$ 4.0σ(F))	1230 ($F >$ 4.0σ(F))	997 ($F >$ 6.0σ(F))	3051 ($F >$ 4.0σ(F))	1649 ($F >$ 4.0σ(F))
T_{min}/T_{max}	n/a	0.522/0.841	0.787/0.924	0.816/0.956	n/a	n/a	0.695/0.949	n/a	n/a	0.797/0.952	0.726/0.917	n/a	0.884/0.926	0.745/0.957	0.714/0.968
Largest difference peak (e Å^{-3})	0.17	0.37	0.32	0.31	0.79	0.31	0.52	0.90	0.38	0.84	0.46	0.32	0.37	0.34	0.31
Largest difference hole (e Å^{-3})	−0.17	−0.58	−0.39	−0.32	−0.36	−0.25	−0.31	−0.49	−0.38	−0.54	−0.30	−0.34	−0.27	−0.27	−0.26
No. of parameters	164	190	208	244	226	71	272	287	244	283	151	151	149	316	178
R [a]	0.0397	0.0351	0.0475	0.0505	0.0780	0.0534	0.0558	0.1002	0.0545	0.0830	0.0565	0.0597	0.0520	0.0501	0.0534
wR [a]	0.0454	0.0488	0.0573	0.0631	0.0976	0.0650	0.0694	0.1267	0.0660	0.1076	0.0657	0.0771	0.0600	0.0584	0.0620
GOF [b]	1.07	1.65	1.90	1.75	1.55	1.25	1.96	1.34	1.84	2.06	1.05	0.99	1.68	1.07	1.70

[a] $R = \Sigma||F_o| - |F_c||/\Sigma|F_o|$; $wR = [\Sigma w(|F_o| - |F_c|)^2/\Sigma w|F_o|^2]^{1/2}$; $w = 1/\sigma^2(F_o) + g^*(F_o)^2$; $g = 0.0008$ for **8**, 0.0005 for **9a**, **9c**-*cis*, **9f**, **11a**, **11h**, and **13h**, 0.002 for **9c**-*trans*, 0.0018 for **11d**, 0.0015 for **9d** and **11d**, 0.005 for **10a**, 0.00175 for **11f**, 0.0035 for **11g**, and 0.00125 for **13b**, respectively.

[b] GOF $= [\Sigma w(|F_o| - |F_c|)^2/(NO - NV)]^{1/2}$, where NO is the number of observations and NV is the number of variables.

Structure solutions and full-matrix least-squares refinements on F were accomplished with the SHELXTL PC package of programs. Heavy atoms were located via direct methods for **8**, **9b**, **9c**-*cis*, **9c**-*trans*, **11a**, **11d**, **11g**, and **13h**, while Patterson maps were employed for **9d**, **9f**, **10a**, **11f**, **11h**, and **13b**. Atomic scattering factors were from the literature [40]. All non-hydrogen atoms were refined anisotropically, with the exceptions of **8** and **10a**. For **8**, only the heteroatoms, methyl carbon atoms of the $SiMe_3$ groups, and the carbon atoms of the *t*-Bu group were refined anisotropically, while for **10a**, only the metal atoms and heteroatoms were refined anisotropically, due to a paucity of data. Hydrogen atom positions were calculated geometrically, fixed at a C–H distance of 0.96 Å, and not refined, with three exceptions. For **8**, the hydrogen atoms bonded to O(2) and O(3) were located and refined. For **9c**-*cis*, the *n*-Pr substituent containing C(13), C(14), and C(15) was disordered. Two positions were located for C(14) and C(15) and refined with equal site occupancies; C(13) was not disordered. Similarly for **9f**, the *i*-Bu substituent containing C(14) through C(17) was disordered. Two positions were located for C(14), C(16), and C(17) and refined with site occupancies of 58/42%; C(15) was not disordered. In both cases, calculated hydrogen atom positions were omitted for the disordered alkyl groups. Crystal data and further data collection parameters for the studied complexes are summarized in Table 5.

5. Supplementary material

Crystallographic data for the structure analyses have been deposited with the Cambridge Crystallographic Data Centre, CCDC no. 202535 for compound **8**, no. 202536 for compound **9a**, no. 202537 for compound **9b**, no. 202538 for compound **9c**-*cis*, no. 202539 for compound **9c**-*trans*, no. 202540 for compound **9d**, no. 202541 for compound **9f**, no. 202542 for compound **10a**, no. 202543 for compound **11a**, no. 202544 for compound **11d**, no. 202545 for compound **11f**, no. 202546 for compound **11g**, no. 202547 for compound **11h**, no. 202548 for compound **13b** and no. 202549 for compound **13h**. Copies of this information may be obtained from The Director, CCDC, 12 Union Road, Cambridge CB2 1EZ, UK (Fax: +44-1233-336033; e-mail: deposit@ccdc.cam.ac.uk or www: http://www.ccdc.cam.ac.uk).

Acknowledgements

We thank the New York State Science and Technology Foundation, Center for Advanced Thin Film Technology, and the Focus Center-New York for Gigascale Interconnects for financial support. We also thank Claudia Birringer and Ester Mahindu for assistance in some of the experimental studies.

References

[1] T.T. Kodas, M.J. Hampden-Smith (Eds.), The Chemistry of Metal CVD, VCH Publishers, New York, 1994.
[2] J.T. Spenser, Prog. Inorg. Chem. 41 (1994) 145.
[3] S.P. Murarka, S.W. Hymes, Crit. Rev. Solid State Mater. Sci. 20 (1995) 87.
[4] T.J. Marks, Pure Appl. Chem. 67 (1995) 313.
[5] P. Doppelt, Coord. Chem. Rev. 178–180 (1998) 1785.
[6] M.J. Hampden-Smith, T.T. Kodas, A. Ludviksson, in: L.V. Interrante, M.J. Hampden-Smith (Eds.), Chemistry of Advanced Materials, Wiley–VCH, New York, 1988, p. 143.
[7] T.N. Theis, IBM J. Res. Develop. 44 (2000) 379.
[8] R.E. Sievers, J.E. Sadlowski, Science (Washington, DC) 201 (1978) 217.
[9] B.D. Fahlman, A.R. Barron, Adv. Mater. Opt. Electron. 10 (2000) 223.
[10] P. Mushak, M.T. Glenn, J. Savory, Fluorine Chem. Rev. 6 (1973) 43.
[11] K.I. Pashkevich, V.I. Saloutin, I.Y. Postovskii, Russ. Chem. Rev. 50 (1981) 180.
[12] P.J. Toscano, C. Dettelbacher, J. Waechter, N.P. Pavri, D.H. Hunt, E.T. Eisenbraun, B. Zheng, A.E. Kaloyeros, J. Coord. Chem. 38 (1996) 319.
[13] M.L. Hitchman, S.H. Shamlian, D.D. Gilliland, D.J. Cole-Hamilton, J.A.P. Nash, S.C. Thompson, S.L. Cook, J. Mater. Chem. 5 (1995) 47.
[14] B. Zorich, Solid State Technol. 41 (1998) 9.
[15] G.S. Girolami, P.M. Jeffries, L.H. Dubois, J. Am. Chem. Soc. 115 (1993) 1015.
[16] K.K. Banger, A. Kornilov, R.U. Claessen, E.T. Eisenbraun, A.E. Kaloyeros, P.J. Toscano, J.T. Welch, Inorg. Chem. Commun. 4 (2001) 496.
[17] (a) R.U. Claessen, J.T. Welch, P.J. Toscano, K.K. Banger, A.M. Kornilov, E.T. Eisenbraun, A.E. Kaloyeros, Mater. Res. Soc. Symp. Proc. 612 (2000) D6.8.1;
(b) Physicochemical characterization gave evidence for smooth, conformal films of essentially pure Cu (as thick as 100 nm) with near bulk resistivity and with only minimal oxygen and carbon contamination and no silicon impurities.
[18] Y. Apeloig, I. Zharov, D. Bravo-Zhivotovskii, Y. Ovchinnikov, Y. Struchkov, J. Organomet. Chem. 499 (1995) 73.
[19] D.I. Gasking, G.H. Whitham, J. Chem. Soc. Perkin Trans. 1 (1985) 409.
[20] J.-B. Verlhac, H. Kwon, M. Pereyre, J. Organomet. Chem. 437 (1992) C13.
[21] J.-P. Bouillon, C. Portella, Tetrahedron Lett. 38 (1997) 6595.
[22] (a) J.T. Welch, P.J. Toscano, R. Claessen, A. Kornilov, K.K. Banger, US Patent 6,184,403 (Cl. C07 F1/8) 2001; Chem. Abstr. 133: 358444.;
(b) R.U. Claessen, A.M. Kornilov, K.K. Banger, C.C Wells, P.J. Toscano, J.T. Welch, in preparation.
[23] R.F. Cunico, C. Kuan, J. Org. Chem. 50 (1985) 5410.
[24] J.A. Soderquist, I. Rivera, A. Negron, J. Org. Chem. 54 (1989) 4051.
[25] A typical Si–C(sp^3) bond length is 1.85 Å: J.E. Huheey, E.A. Keiter, R.L. Keiter, Inorganic Chemistry: Principles of Structure and Reactivity, vols. A-30, fourth ed., Harpercollins College Publishers, New York, 1993.
[26] A.G. Brook, Adv. Organomet. Chem. 7 (1968) 95.
[27] A.G. Brook, J.M. Duff, P.F. Jones, N.R. Davis, J. Am. Chem. Soc. 89 (1967) 431.

[28] T.J. Wenzel, E.J. Williams, R.C. Haltiwanger, R.E. Sievers, Polyhedron 4 (1985) 369.
[29] D.V. Soldatov, J.A. Ripmeester, S.I. Shergina, I.E. Sokolov, A.S. Zanina, S.A. Gromilov, Yu.A. Dyadin, J. Am.Chem. Soc. 121 (1999) 4179.
[30] W.H. Watson, W.W. Holley, Croat. Chem. Acta 57 (1984) 467.
[31] S. Sans-Lenain, A. Gleizes, Inorg. Chim. Acta 211 (1993) 67.
[32] S. Patnaik, T.N. Guru Row, L. Ragunathan, A. Devi, J. Goswami, S.A. Shivashankar, S. Chandrasekaran, W.T. Robinson, Acta Crystallogr. Sect. C: Cryst. Struct. Commun. 52 (1996) 891.
[33] P.C. Chieh, J. Trotter, J. Chem. Soc. A (1969) 1778.
[34] R.W. Harrison, J. Trotter, J. Chem. Soc. A (1968) 258.
[35] S.I. Troyanov, N.P. Kuz'mina, M.Yu. Khudyakov, L.I. Martynenko, Russ. J. Coord. Chem. 20 (1994) 60.
[36] M.J. DelaRosa, P.J. Toscano, J.T. Welch, unpublished results.
[37] M.L. Connolly, J. Mol. Graphics 11 (1993) 139.
[38] W.C. Still, M. Kahn, A. Mitra, J. Org. Chem. 43 (1978) 2923.
[39] A. Bruce, J.L. Corbin, P.L. Dahlstrom, J.R. Hyde, M. Minelli, E.I. Stiefel, J.T. Spence, J. Zubieta, Inorg. Chem. 21 (1982) 917.
[40] D.T. Cromer, J.B. Mann, Acta Crystallogr. Sect. A 24 (1968) 321.